nanomaterials

MDPI

Review

Transition Metal Oxide Electrode Materials for Supercapacitors: A Review of Recent Developments

Ruibin Liang [1], Yongquan Du [1], Peng Xiao [1,2,*], Junyang Cheng [1], Shengjin Yuan [1], Yonglong Chen [1], Jian Yuan [1,2] and Jianwen Chen [3]

[1] School of Physics and Optoelectronic Engineering, Foshan University, Foshan 528000, China; leungseoiban@163.com (R.L.); du_0258@163.com (Y.D.); cheng-jy@outlook.com (J.C.); ysj981006@163.com (S.Y.); c19875916364@163.com (Y.C.); yuanjian054@163.com (J.Y.)

[2] Guangdong-Hong Kong-Macao Joint Laboratory for Intelligent Micro-Nano Optoelectronic Technology, Foshan University, Foshan 528225, China

[3] School of Electronic and Information Engineering, Foshan University, Foshan 528000, China; iamjwen@126.com

* Correspondence: xiaopeng@fosu.edu.cn

Abstract: In the past decades, the energy consumption of nonrenewable fossil fuels has been increasing, which severely threatens human life. Thus, it is very urgent to develop renewable and reliable energy storage devices with features of environmental harmlessness and low cost. High power density, excellent cycle stability, and a fast charge/discharge process make supercapacitors a promising energy device. However, the energy density of supercapacitors is still less than that of ordinary batteries. As is known to all, the electrochemical performance of supercapacitors is largely dependent on electrode materials. In this review, we firstly introduced six typical transition metal oxides (TMOs) for supercapacitor electrodes, including RuO_2, Co_3O_4, MnO_2, ZnO, XCo_2O_4 (X = Mn, Cu, Ni), and $AMoO_4$ (A = Co, Mn, Ni, Zn). Secondly, the problems of these TMOs in practical application are presented and the corresponding feasible solutions are clarified. Then, we summarize the latest developments of the six TMOs for supercapacitor electrodes. Finally, we discuss the developing trend of supercapacitors and give some recommendations for the future of supercapacitors.

Keywords: energy storage devices; supercapacitors; transition metal oxides; developing trend

Citation: Liang, R.; Du, Y.; Xiao, P.; Cheng, J.; Yuan, S.; Chen, Y.; Yuan, J.; Chen, J. Transition Metal Oxide Electrode Materials for Supercapacitors: A Review of Recent Developments. *Nanomaterials* **2021**, *11*, 1248. https://doi.org/10.3390/nano11051248

Academic Editor: Jung-Sang Cho

Received: 12 April 2021
Accepted: 4 May 2021
Published: 10 May 2021

1. Introduction

Owing to the rapid development of the global economy, accelerating the consumption of fossil fuels like coal, fuel, and natural gas, the problems of global climate change and environmental pollution are increasing to significant levels. Developing solar, wind, tidal, and other renewable clean energy is a way to mitigate current energy and environmental pollution problems [1–6]. However, those renewable clean forms of energy are severely restricted by environmental factors and energy supply is intermittent [7]. Therefore, it is urgent to develop effective and reliable devices for energy storage [8,9]. As a new type of storage device, supercapacitors have gained great attention in recent years thanks to their advantages of fast charge/discharge rate, high power density, and very long cycle life [10–14]. Supercapacitors have great potential in the area of portable electronic equipment, renewable energy systems, and hybrid power cars [15–17]. There are two categories of supercapacitors: electrical double-layer capacitors (EDLCs) and pseudocapacitors [18,19]. For EDLCs, energy is stored with the charge accumulating on the interface between the electrode and electrolyte. For pseudocapacitors, the energy is stored through a fast and reversible faradaic redox reaction [20–22]. At present, the low energy density is still the bottleneck of supercapacitors [23,24]. According to the energy density formula, $E = \frac{1}{2} \times C \times V^2$, where E represents the energy density, C represents the specific capacitance, and V represents the potential window, we can know that the energy density of a

supercapacitor depends on both capacitance and operating voltage, and it can be enhanced by increasing the potential window and using an electrode material with high capacitance [25,26]. It is noteworthy that the design and preparation of electrode materials are the key steps to determine the electrochemical performance of supercapacitors. In other words, the performance of supercapacitors is highly dependent on electrode materials [27–30].

Electrode materials can be divided into three categories: carbon materials, conductive polymers, and transition metal oxides (TMOs). Carbon materials are usually used as electrode materials for EDLCs. They have the characteristics of high specific surface area, adjustable pore size distribution, and excellent electrical conductivity [31,32]. Owing to the storage mechanism of EDLCs, carbon materials can provide high power density, but low energy density, which limits the overall performance [33,34]. Carbon materials such as graphene, carbon nanotubes, and carbon nanofibers have been widely studied for electrode materials. However, low specific capacitance of carbon material limits the capacity of the EDLCs [35], and the applications of those carbon materials are limited by their high cost [36]. The conductive and pseudocapacitive properties of conductive polymers are good, but the stability is poor, and conductive polymers can easily fall off the substrate [37,38]. For example, the charge and discharge speed of polyaniline is low and the stability of the charge/discharge process is poor [39,40]. TMOs have higher specific capacitance (100–2000 F g^{-1}), higher energy density than carbon materials, and better chemical stability than conductive polymers [41–43]. Thanks to its high theoretical capacitance and rapid faraday redox reaction, RuO_2 is thought to be an optimal pseudocapacitive electrode material [44–46]. However, its high price and toxicity to the environment seriously hinder its application in supercapacitors [47–49]. Co_3O_4, MnO_2, and ZnO have the advantages of being natural abundant and high specific capacitance, which makes them substitutes for RuO_2 [50,51]. The disadvantage of poor electrical conductivity is exhibited by many metal oxide electrodes [52]. Because of the co-existence of two metal ions and synergistic effects of elements, ternary metal oxides, AB_2O_4 (A or B = Ni, Co, Mo, Mn, and so on), have more active reaction sites and high electrical conductivity than binary metal oxides [53]. In addition, spinel cobaltates (XCo_2O_4, X = Ni, Cu, Zn, Mn, and so on) and metal molybdate ($AMoO_4$, A = Ni, Mn, Co, and so on) have received tremendous research interest because of their low cost, enhanced electrochemical activity, and being a natural abundant resource [54,55].

In this review, six transition metal oxide materials including RuO_2, Co_3O_4, MnO_2, ZnO, XCo_2O_4 (X = Mn, Cu, Ni), and $AMoO_4$ (A = Co, Mn, Ni, Zn) are firstly introduced. Secondly, existing problems of those TMOs in practical application and the corresponding methods are presented. The methods include synthesizing composites, preparing material in nano scale, introducing battery-type material or oxygen vacancies, and modification of quantum dots. Particularly, we introduce the latest developments of six TMOs for supercapacitor electrode according to the strategies. Finally, the future development of supercapacitors is discussed and recommendations on supercapacitors are exhibited.

2. TMOs-Based Electrode Materials

2.1. RuO_2

RuO_2 has high theoretical capacitance (2000 F g^{-1}) and it can carry out rapid faraday redox reaction. It has good electrical conductivity, high chemical and thermal stability, as well as a big voltage window. Thus, RuO_2 is called the most ideal pseudocapacitive electrode material [40,56]. However, ruthenium is too expensive to be used for large-scale synthesis of electrode materials.

2.1.1. RuO_2-Based Composite Electrodes

Synthesizing composites can improve the utilization of RuO_2 and reduce the cost of RuO_2 electrode [57]. At the same time, the synergistic effect of the materials is beneficial to improve the electrochemical performance of the electrode. Various forms of RuO_2-based electrodes have been prepared such as metal sulfide-RuO_2 electrode, metal

oxide-RuO_2 electrode, carbon material-RuO_2 electrode, and multicomponent RuO_2-based electrode [39,57–61]. Asim et al. [62] decorated carbon nanotubes (CNTs) grown carbon cloth (CNTS-CC) with RuO_2 nanorods (RuO_2-NRs) via chemical vapor deposition (CVD) and the annealing process. The prepared electrode has the characteristics of both supercapacitors and lithium batteries. The results show that the designed material has high specific capacitance (176 F g^{-1}) and superior cycling stability (97% retention after 10,000 cycles at 40 mA cm^{-2}) (Figure 1).

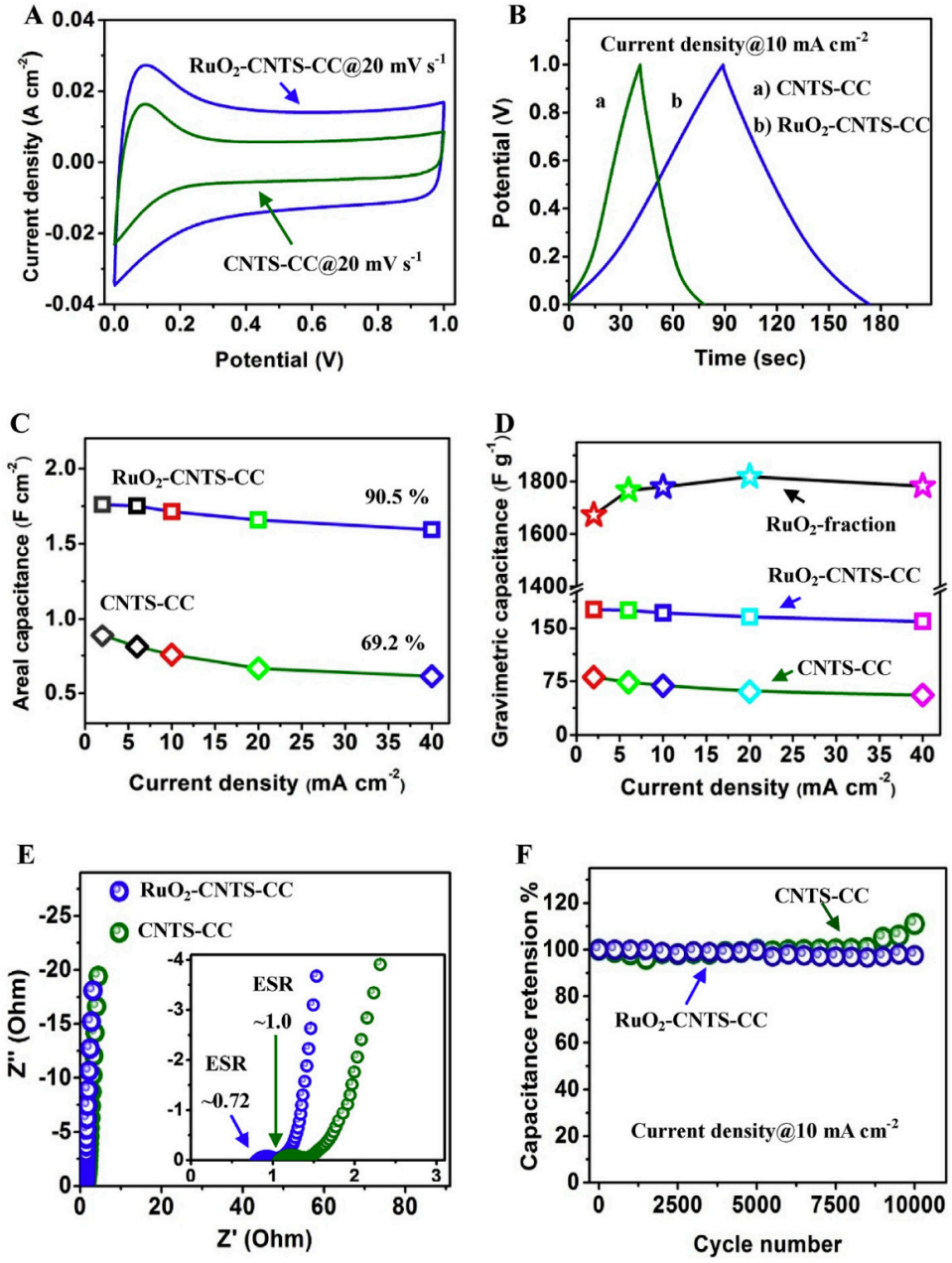

Figure 1. Electrochemical performance of different electrodes in liquid state supercapacitors using 1 M H_2SO_4 electrolytes: (**A**) comparison of CV at 20 mV s^{-1}; (**B**) GCD curves at 10 mA cm^2; (**C**) calculated areal capacitance at a range of current densities; (**D**) calculated gravimetric capacitance at different current densities; (**E**) Nyquist plots of different samples, and the inset showing the corresponding magnified high-frequency regions; and (**F**) cyclic stability over 10,000 cycles at 10 mA cm^{-2}. Reproduced with permission from [62]. Copyright 2019 Elsevier. CNTS-CC, carbon nanotubes grown carbon cloth. CV, cyclic voltammetry. GCD, galvanostatic charge-discharge. ESR, equivalent series resistance.

In addition, they demonstrate a reversible capacity of ~3.85 mAh cm^{-2} at the current density of 100 mA cm^{-2} as a Li-ion batteries electrode. The excellent electrochemical performance lies in the synergistic effect of metal oxide NRs and the unique structure of CNTS-CC. Enlarged surface area and exposed active sites allow accessibility of the ions/electrolytes to the electrodes. Ternary single-walled carbon nanotubes/RuO_2/polyindole (SWCNT/RuO_2/PIn) nanocomposite fabricated by Zhu's group [63] presents the specific capacitance of 1283 F g^{-1} at 1.0 A g^{-1}. At 500 W kg^{-1} and 5000 W kg^{-1}, the energy densities of the SWCNT/RuO_2/PIn electrode-based symmetric supercapacitor are 42 W h kg^{-1} and 33 W h kg^{-1}, respectively. It also shows good cycling stability and capacitive performance of 1203 F g^{-1} at 1.0 A g^{-1}. Via the hydrothermal and annealing process, $CuCo_2O_4$/CuO nanoneedles were synthesized directly on the conductive Ni foam (NF), on which RuO_2 nanoparticles were deposited [64]. The $CuCo_2O_4$/CuO@RuO_2 can work as water oxidation catalysis and has low overpotential (279 mV at 10 mA cm^{-2}), low Tafel slope, and stable long-term performance. Besides, it achieves a high areal capacity up to 862.5 mAh cm^{-2} and a capacity retention of about 90.1% after 8000 cycles. The hybrid supercapacitor fabricated by $CuCo_2O_4$/CuO@RuO_2 and activated carbon achieves an energy density of 0.84 mW h cm^{-2} at 8 mW cm^{-2}.

2.1.2. Hydrographic RuO_2

In the reports above, many electrode materials have the addition of carbon materials. Theoretically, adding carbon materials can improve the surface area and conductivity of electrodes [65]. However, some reports pointed out that the porous surface of carbon materials was blocked by RuO_2 particles, which results in reduced surface area, limited electrochemical properties, and decreased double layer capacitance [66,67]. Hydrated RuO_2 is a kind of nanocrystalline material with RuO_2 as the core and a small amount of water hydrogen bond on the surface. The form of porous structure provides conduction paths for protons to enter the inner part of RuO_2 [68,69]. The annealing treatment of activated carbon-RuO_x•nH_2O composites (annealing for 2 h in 200 °C air) obviously improves the discontinuity of the electron path in particles. Further, the obstacle of electron hopping between particles is reduced because a large amount of active carbon (AC) powder is introduced. The specific capacitance of the RuO_x•nH_2O is 1340 F g^{-1} (at 25 mV s^{-1}) [70]. Similarly, Yang's group [71] synthesized RuO_2@SWCNTs/graphene (S/G) composites by the sol–gel method. The hybrid electrode material, RuO_2@S/G-60, has a specific capacitance up to 988 F g^{-1} and excellent rate capability at 1 A g^{-1}. Hexagon WO_3 (h-WO_3) and hydrous RuO_2 were respectively prepared on three-dimensional conducting carbon cloth (CC) via the hydrothermal method [72], which meant fast electronic pathway, high conductivity substrate, high surface area, and enhanced electrochemical performance. Figure 2a–d shows the field emission scanning electron microscopy (FE-SEM) images, transmission electron microscope (TEM) image, and high resolution transmission electron microscope (HRTEM) image of hydrous RuO_2 at different magnifications. Figure 2e–h shows the FE-SEM images, TEM image, and HRTEM image of h-WO_3 at different magnifications.

The asymmetric supercapacitor was fabricated in H_2SO_4 aqueous electrolyte with h-WO_3/CC as negative electrode and hydrated RuO_2/CC as positive electrode. At an operating voltage of 1.6 V, the asymmetric supercapacitor device is optimized with volumetric capacitance of 3.52 F cm^{-3} at 5 mA cm^{-2}. Moreover, at a power density of 40 W cm^{-3}, the asymmetric supercapacitor device shows brilliant energy density of 1.25 W h cm^{-3} and it also shows promising electrochemical stability. By comparison, an all-pseudocapacitive asymmetric device [73] has an energy density of only 37 μW h cm^{-2} at 40 mW cm^{-2}, but a remarkable 96% retention after 20,000 charge/discharge cycles.

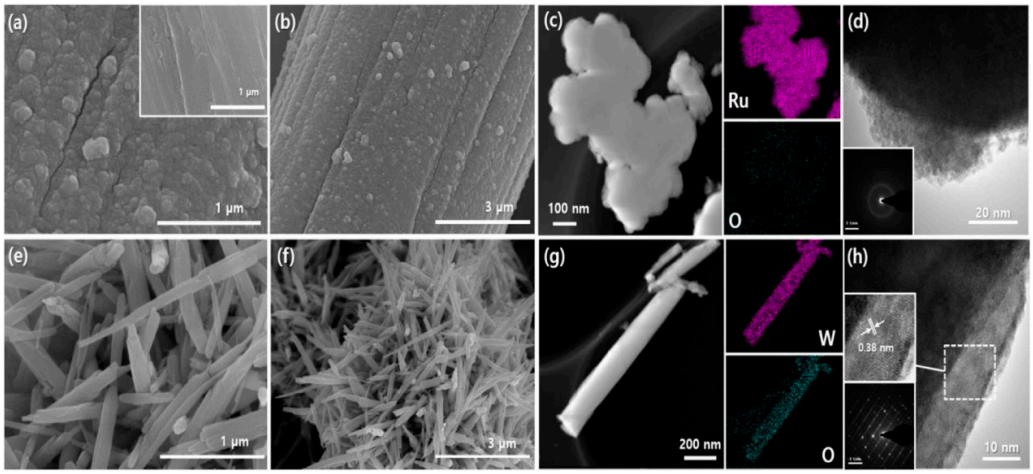

Figure 2. (**a**,**b**) Inset of (**a**) FE-SEM images of hydrous RuO_2 on carbon cloth at different magnifications; (**c**) TEM image of the hydrous RuO_2 and its EDS mapping; (**d**) HRTEM image of hydrous RuO_2 and its SAED pattern in the inset of (**d**); (**e**,**f**) FE-SEM images of h-WO_3 on carbon cloth at different magnifications; (**g**) TEM image of the h-WO_3 nanorod and its EDS mapping; (**h**) HRTEM image of h-WO_3 nanorod. The inset shows the SAED pattern, reproduced with permission from [72] Copyright 2019 Elsevier. FE-SEM, field emission scanning electron microscopy. TEM, transmission electron microscope. EDS, energy dispersive X-ray spectroscopy. HRTEM, high resolution transmission electron microscope. SAED, selected area electron diffraction.

2.2. Co_3O_4

Co_3O_4 is a kind of transition metal oxide belonging to the spinel family, and the faradic redox reaction of Co_3O_4 can be described as follows [74]:

$$Co_3O_4 + OH^- \leftrightarrow 3CoOOH + e^- \quad (1)$$

$$CoOOH + OH^- \leftrightarrow CoO_2 + H_2O + e^- \quad (2)$$

Co_3O_4 has the advantages of high theoretical specific capacitance (3560 F g^{-1}), low price, environmental friendliness, and good chemical durability, so it is a promising active material [75–77]. However, the capacitance in practical application differs a lot from the theoretical value. A reason is that electron transfer is hindered owing to low conductivity, slow kinetics, large volume expansion-contraction, and severe particle aggregation. Thus, the capacitance and cycling performance of Co_3O_4 are limited [78,79].

2.2.1. Co_3O_4 Nanomaterials

Nanomaterials have a large surface with numerous active sites. The ultra-small size of nanomaterials shortens the electron/ion diffusion path, providing favorable transfer pathways [78]. Because the dimension and morphology of the materials play an important role in improving the electrochemical performance, increasingly more attention has been paid to the synthetic materials in micro and nano scale [80]. A variety of Co_3O_4 nanomaterials have been synthesized, such as nanowires [81], nanofibers [82], nanoparticles [83,84], and nanosheets [85]. Yue and co-workers [86] used a simple and environmentally friendly one-step hydrothermal and calcination method to prepare Co_3O_4/reduced graphene oxide (rGO) composites. Tiny Co_3O_4 nanoparticles are dispersed on rGO flakes and a three-dimensional structure is formed. The prepared electrode has more active sites than Co_3O_4 nanowires [87] to achieve better electrochemical performance. The optimized electrode Co_3O_4/rGO-120-12 shows high specific capacitance of 1152 F g^{-1} at 1 A g^{-1}. Indira Priyadharsini [88] firstly prepared Co_3O_4 nanoparticles by the sol–gel method. The obtained Co_3O_4 nanoparticles, carbon, and polyvinylidene fluoride (PVDF) were then mixed with a mass ratio of 8:1:1. The electrode was prepared by coating the synthesized slurry uniformly on the Ni foam substrate. The specific capacitance of the electrode at 11 mA cm^{-2} is

761.25 F g^{-1}. The reason for the low specific capacitance is that the addition of PVDF increases the resistance between the collector and the redox active material, which results in a decrease in the number of active sites and the electron/charge transport rate [89]. However, directly growing Co_3O_4 active materials on conductive substrates such as carbon fiber, carbon cloth, stainless steel sheet, and metal foam can avoid the addition of binder and conductive additive [51]. Ag doped Co_3O_4 nanosheets synthesized on Ni foam [90] possess a specific surface area (176 m^2 g^{-1}) larger than the original Co_3O_4 (108 m^2 g^{-1}). There is still a superior specific capacitance of 1323 F g^{-1} at the current density of 10 A g^{-1} (92.84% of the initial specific capacitance), indicating outstanding rate capability of the sample. Furthermore, it exhibits 104.7% of the initial capacitance at the first 2000 cycles. The electrode materials prepared by Yang's group [91] and Wang et al. [92] both show good electrochemical properties (883 F g^{-1} and 1606.6 F g^{-1} at the current density of 1 A g^{-1}, respectively). Electrode prepared by Wei [93] has unique nanoarray structures. The SEM images of Co_3O_4/NF with different heating times are shown in Figure 3a–i. Figure 3j–l shows the element mapping images of Co_3O_4 nanoflakes.

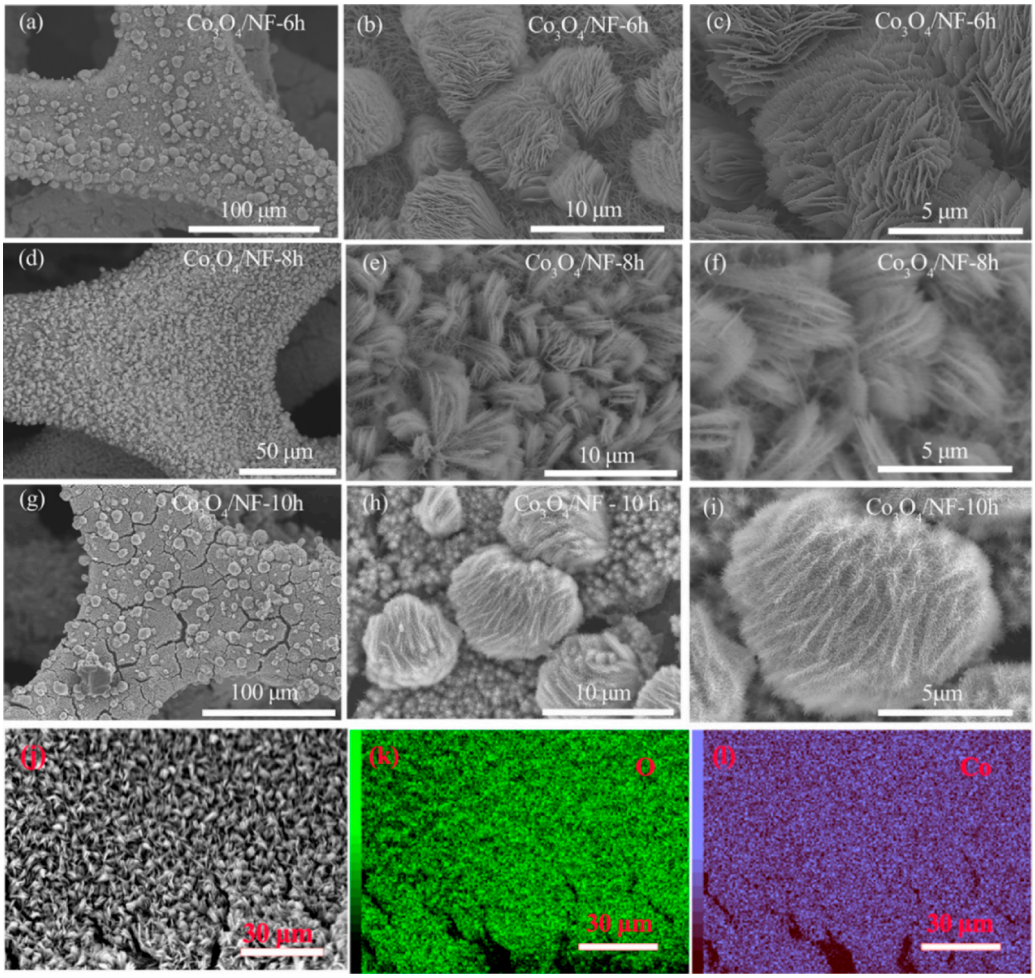

Figure 3. SEM images: (**a–c**) Co_3O_4/nickel foam (NF)—6 h; (**d–f**) Co_3O_4/NF—8 h; (**g–i**) Co_3O_4/NF—10 h; (**j–l**) element mapping images of Co_3O_4 nanoflakes, reproduced with permission from [93] Copyright 2021 Elsevier. NF, Ni foam.

Co_3O_4 nanowires were anchored on the surface of the Co_3O_4 nanosheet, effectively expanding the surface area, providing rich active states for the faradaic redox reaction and promoting the diffusion rate of electrolyte ions. The sample prepared at hydrothermal heating for 8 h (Co_3O_4/NF-8 h) shows a high specific capacitance of 2053.1 F g^{-1} at 1 A g^{-1}. The working voltage of the hybrid supercapacitor device assembled by the hetero-

structured Co_3O_4 array and graphene can reach 1.6 V. The maximum energy density of 22.2 W h kg^{-1} is delivered and the excellent cycle is proved by the 93.3% capacitance retention after 10,000 cycles.

2.2.2. A Strategy for Preparation of Co_3O_4 Nanomaterials

In recent years, metal organic frameworks (MOFs)-based materials have attracted attention in various fields of gas adsorption, energy device, pollutant degradation, electrocatalysis, and drug release [1]. Besides, with adjustable porous structure, controllable pore size distribution, and high surface area, MOFs are thought to be an ideal template for the preparation of Co_3O_4 nanomaterials [94,95]. Commonly, Zeolitic Imidazolate Frameworks-67 (ZIF-67) is used as precursor to synthesize Co_3O_4 nanomaterials. With ZIF-67 crystals as precursor, porous Co_3O_4 nanoparticles [96] were transformed by simple calcination treatment. The results show that ZIF-67-derived Co_3O_4 nanoparticles exhibit high specific capacitance (190 F g^{-1} at 5 A g^{-1}) and capacitance retention (71.42% after 5000 cycles). Bao and co-workers [97] used ZIF-67 as a template and successfully constructed a series of Co_3O_4 embedded α-Co/$Ni(OH)_2$ hollow nanocages. The prepared composite (α-Co/$Ni(OH)_2$@Co_3O_4-70) has abundant electrolyte diffusion channels and reactive active sites. At the same time, it possesses excellent conductivity and stability. Therefore, the high capacitance of 1000 F g^{-1} is obtained at 1 A g^{-1} and the capacitance retention is 74% at 10 A g^{-1}. Meanwhile, the hybrid nanocages still maintain 72.34% of original capacitance after 8000 charge/discharge cycles. In addition, α-Co/$Ni(OH)_2$@Co_3O_4-70//active carbon (AC) device has an energy density of 23.88 W h kg^{-1} at a power density of 0.075 kW kg^{-1}. Wei et al. [98] developed a novel method (bottom-up approach) to synthesize ZIF-67 nanosheets. The ZIF-67 is in situ converted into Co_3O_4 ultrathin nanoparticles by thermal treatment. The energy density at 790.7 W kg^{-1} of asymmetric supercapacitors prepared with Co_3O_4//AC is 46.5 W h kg^{-1}. Moreover, the overpotential of 2D Co_3O_4 ultrathin nanoparticles at the onset potential is 230 mV and Tafel slope is 74.0 mV dec^{-1}. This shows 2D Co_3O_4 ultrathin nanoparticles' great performance in oxygen evolution reaction. Besides, Co-based MOFs (Co-MOFs) have become fascinating templates for thermal transformation to generate porous Co_3O_4 structures [99]. Li et al. [100] prepared 3D porous carbon (3DPC)/Co_3O_4 composites by pyrolysis of 3D graphene/Co-MOF precursor. The electrochemical performance of the composites is not good (specific capacitance of 423 F g^{-1} at 1 A g^{-1} and capacitance attenuation of about 17% after 2000 cycles). This is because MOFs-based electrodes are usually composed of insulation binder, conductivity additives, and MOFs, which hinders the electrolyte penetration and reduces the electron transport between electroactive sites of active material and electrolytes [101].

2.2.3. Electrode Materials on Conductive Substrates

Synthesizing electrode materials directly on conductive substrates can avoid the addition of insulation binder so as to reduce interparticle resistance [51]. In order to further obtain high performance electrode materials, Han et al. [102] synthesized petal-like Co_3O_4@$CoNi_2S_4$ nano-wall arrays on carbon cloth. The synergistic effect of Co-MOF-derived Co_3O_4 skeleton is utilized to improve the electrochemical activity of cobalt nickel sulfide. The specific capacitance of the Co_3O_4@$CoNi_2S_4$ electrode is 244.4 mAh g^{-1} at 1 A g^{-1} and a specific capacitance attenuation of 18.7% at 16 A g^{-1}. At a power density of 884.4 W kg^{-1}, the energy density of the Co_3O_4@$CoNi_2S_4$//AC device reaches 55.6 W h kg^{-1}. After 10,000 cycles, the capacitance retention of Co_3O_4@$CoNi_2S_4$ reaches 86%. Liao and co-workers [77] prepared Co_3O_4 nanoparticles on graphene nanosheets supported by carbon fabric. The electrode shows an unbelievable specific capacitance of 3480 F g^{-1}, which is close to the theoretical value (3560 F g^{-1}). Besides, they fabricated a flexible symmetric supercapacitor device with two pieces of prepared electrode. The flexible supercapacitor has no sacrifices of electrochemical performance when it is bent under bending angles from 0° to 150°. Furthermore, the supercapacitor delivers capacitance

of 580 F g^{-1} and 13.8% capacitance decline after 20,000 cycles. The maximum energy density of the device is 80 W h kg^{-1} (Figure 4).

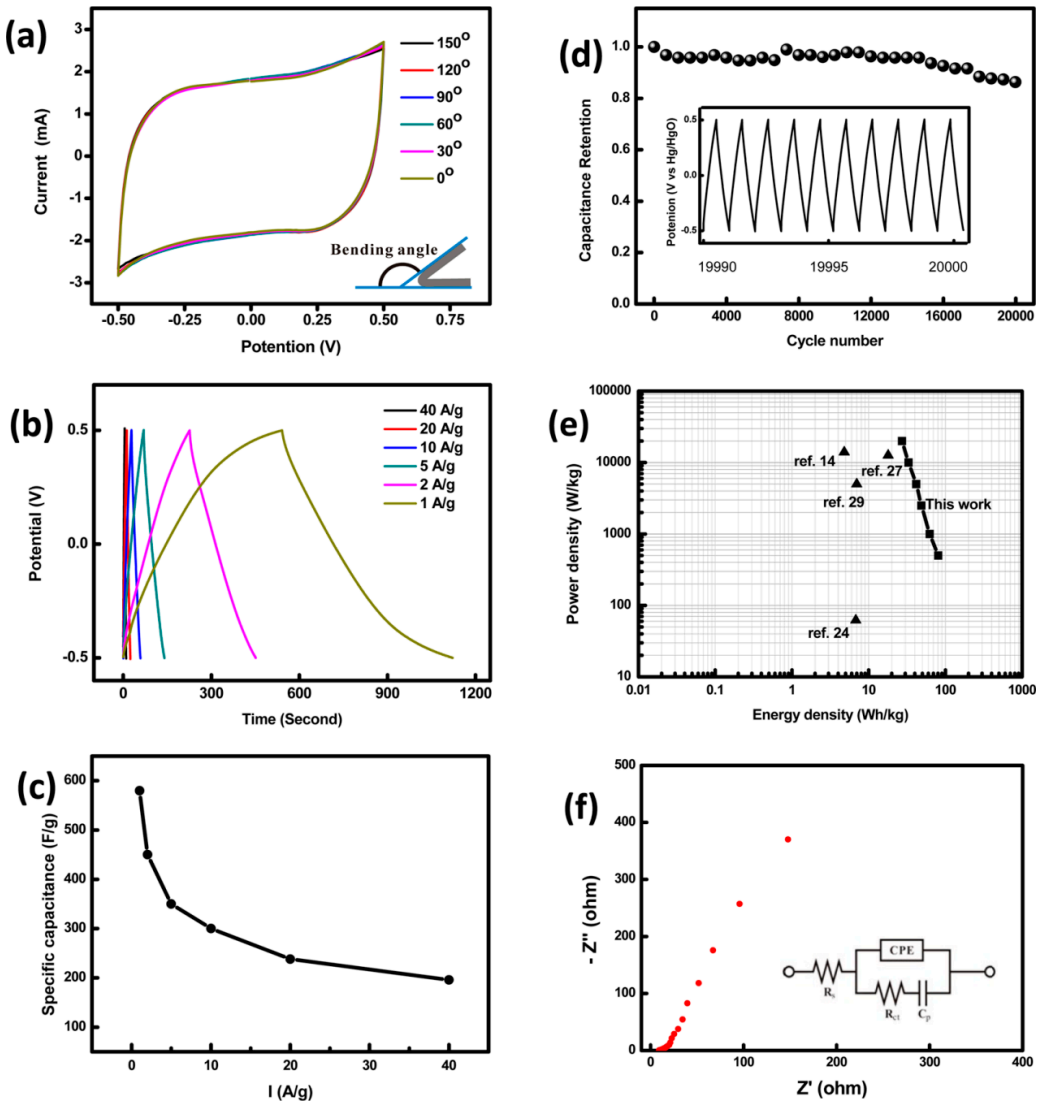

Figure 4. (**a**) CVs curve of the device at different bending angles; (**b**) GCD curves of the supercapacitor device at different current densities; (**c**) specific capacitance vs. current densities for the supercapacitor device; (**d**) cycling stability of the device at 20 A g^{-1}. The inset shows the GCD curves of the last 10 cycles; (**e**) Ragone plots of the supercapacitor device in comparison with other reported supercapacitors; (**f**) Nyquist plot of the supercapacitor device, the inset is the equivalent circuit, reproduced with permission from [77]. Copyright 2015 ACS.

2.3. MnO_2

Owing to its rich natural content, no environmental pollution, and high theoretical specific capacitance (1380 F g^{-1}), MnO_2 has been widely studied as the most competitive transition metal oxide [103–105]. However, its application in supercapacitors is seriously affected because of its poor conductivity and slow ion transport rate [106–108].

2.3.1. Carbon Materials@MnO_2 Composite Electrode

Carbonaceous materials have excellent electrical conductivity and stability with large surface area [31,32]. Carbon nanotubes [109,110], graphene [111,112], carbon nanowires [113,114], carbon nanofibers [115], and other carbon materials can be used as scaffolds for depositing MnO_2 nanostructures. Large surface area with a great quantity of active sites is provided

and the contact path between electrode materials and electrolytes is shortened, which enhances electrochemical properties [116]. The hollow N-doped carbon (HNC)@MnO_2 3D core–shell composites prepared by Cai et al. [117] exhibit a good electrochemical capacity of 247.9 F g^{-1} at 0.5 A g^{-1}, as well as a retention capacity of 82.9% at 5 A g^{-1} after 2000 cycles. Via a simple one-step water bath at 40 °C, Long et al. [118] developed interconnected δ-MnO_2 nanosheets flexible electrode on activated carbon cloth. The electrode displays brilliant charge storage performance (a neglected degradation during the 2000 times of folding). When the power density of the asymmetric supercapacitor is 1198.4 W kg^{-1}, the energy density can reach 49.8 W h kg^{-1}. After 5000 cycles, the capacitance retention of the asymmetric supercapacitor can reach 90.6%. Lei and co-workers [119] synthesized MnO_2 nanosheets@graphenated CNTs network on 316 L stainless steel by the CVD method followed by annealing treatment (Figure 5).

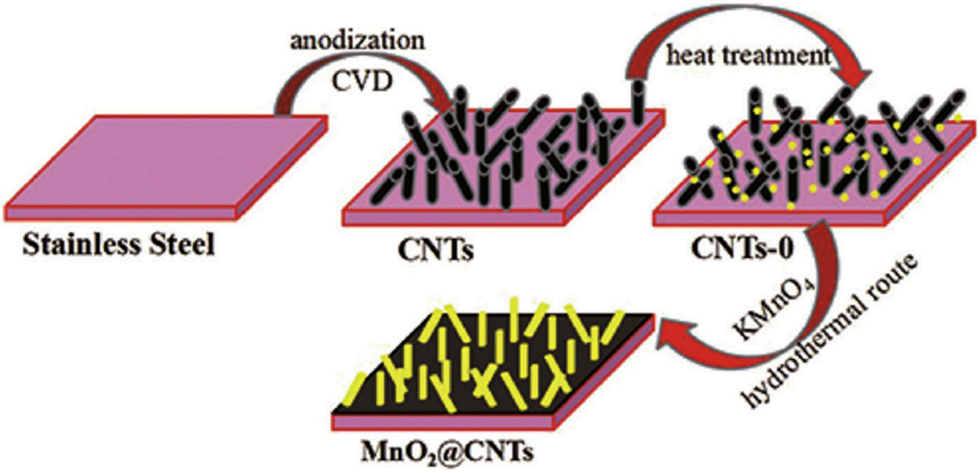

Figure 5. Schematic fabrication of core–shell MnO_2@CNTs composite electrodes on stainless steel. Reproduced with permission from [119]. Copyright 2020 Elsevier.

Providing an effective electronic pathway, graphenated CNTs are interconnected to form porous structures, with MnO_2 nanoparticles uniformly distributed on the surface. Furthermore, the unique structure of MnO_2 nanosheets@graphenated CNTs nanocomposites shortens the ion transport distance, promotes charge transfer, and accelerates reversible redox reactions, thereby improving the capacitance performance. A high energy density of 51.2 W h kg^{-1} is obtained at 24.42 W h cm^{-2} and the maximum power density is 0.4 kW kg^{-1} (200 W cm^{-2}). 3D-graphene/MnO_2 foam composite [120] was prepared by a combination of the CVD and hydrothermal method. The study shows that 3D-graphene/MnO_2 composite electrodes in the absence of carbon black have a high specific capacitance of 333.4 F g^{-1} at 0.2 A g^{-1} and excellent cycling stability.

However, the high cost and complex preparation process of commercial carbon materials are not conducive to large-scale preparation. Therefore, it is very important to develop low price and renewable materials to meet the increasing demand. Biomass resource is a renewable resource with high utilization value. Biomass resource utilization has become a hot area and pillar of economic and social development in the future [121]. Biomass-derived carbon has the advantages of high natural abundance, environmental friendliness, diverse structures, long cycle life, and low costs [36,122,123]. In addition, the multistage pore structure and the inherent stability of carbon materials give biomass carbon unique advantages and prospects in the application of electrochemical materials. Hence, biomass-derived carbon has great potential in supercapacitors. Yang's group [35] used banana peel as a carbon source to synthesize MnO_2/biomass-based porous carbon (BPC) composites by the hydrothermal method. The MnO_2/BPC composites electrode has a great specific capacitance of 139.6 F g^{-1} at the current density of 300 mA g^{-1} and 70 F g^{-1} at 10 A g^{-1}. In addition, it loses 7.7% of the specific capacitance after 1000 cy-

cles. In Shen's research [124], soybean pod was used as the precursor of carbon matrix to prepare MnO_2/soybean pod carbon (SPC) composites by a one-step in situ hydrothermal method. The prepared material retains the original tubular structure of the pods, with a large number of δ-MnO_2 nanorods covered on the surface. According to the research, the MnO_2/SPC electrode has a better specific capacitance than the MnO_2 electrode (530 F g^{-1} and 362 F g^{-1}, respectively). Besides, the symmetric MnO_2/SPC-based supercapacitor displays high capacitance retention of 91% after 6000 cycles and maintains the energy density of 35.1 W h kg^{-1} at a high power density of 9000 W kg^{-1}. The hollow structure of MnO_2/carbon spheres (CSs) [125] was prepared by a simple one-step hydrothermal method. First, 60 mg hollow carbon was dispersed in 30 mL 20 mM $KMnO_4$ aqueous solution by sonication. Then, this aqueous solution was heated at 160 °C for 3 h in a Teflon-lined stainless steel autoclave. After the reaction and cooling down, the product was vacuum filtered, washed, thoroughly dried at 60 °C, and then labeled as MnO_2/hollow CS-20. An asymmetrical supercapacitor is assembled with the MnO_2/hollow CS-30 material as the positive electrode and the hollow CS as the negative electrode. At the 2.0 V voltage window, the maximum energy density (41.4 W h kg^{-1}) is obtained at a power density of 500 W kg^{-1}. Moreover, the asymmetric supercapacitor shows a good cycling stability of 93.9% capacitance retention after 5000 cycles.

2.3.2. Introduction of Battery-Type Metal Oxides

According to Nie's study [126], introducing battery-type metal oxides into MnO_2-based electrodes has been thought to be an effective way to increase the capacity and energy density of supercapacitors. Rapid redox reactions and synergistic effects of MnO_2 and battery metal oxides improve the overall performance of the electrode. The electrode [127] obtained by depositing MnO_2 on NiO nanosheets for 30 min has an ultra-high specific capacitance of 1227.2 F g^{-1} (at 10 A g^{-1}) and a capacitance retention rate of 76.7% after 10,000 cycles. Via a low temperature facile chemical bath deposition, Liu et al. [128] fabricated leaf-like Co_3O_4@MnO_2 nanosheets on the carbon cloth fibers (Co_3O_4@MnO_2CC) with a hierarchical core–shell structure. The leaf-like Co_3O_4@MnO_2 nanosheets exhibit brilliant electrochemical performance, including super-high specific capacitance (616.7 F g^{-1} at 2 A g^{-1}) and superior cyclic stability (83.1% retention after 10,000 cycles at 20 A g^{-1}) as well as high output potential of 1.2 V. The asymmetric supercapacitor (Co_3O_4@MnO_2CC-90 as the cathode and AC as the anode) has energy density of 54.71 W h kg^{-1} at the power density of 1.06 kW kg^{-1} and 86.3% retention of specific capacitance after 10,000 cycles at 10 A g^{-1}.

2.4. ZnO

Electrode materials largely determine the performance of supercapacitors [129]. Therefore, people have been looking for electrode materials with good electrochemical performance. TMOs have gotten extensive attention because of their high redox activity, good theoretical capacitance, and low costs [130]. ZnO is a well-known active material that has the characteristics of environmental protection, natural abundance, and ideal capacitance [50,131,132]. Via the chemical coprecipitation method, Dhivya Angelin et al. [133] modified the ZnO nanostructure with doping Zr. The experimental results indicate that 9 wt.% Zr-doped ZnO nanostructure has the best electrochemical performance of excellent specific capacitance of 518 F g^{-1} (at 1 A g^{-1}) and capacitance retention of 94% (5000 successive galvanostatic charge-discharge cycles). ZnO nanomembranes (NMs) [134] were prepared with 100 atomic layer deposition (ALD) cycles. Figure 6a shows the fabrication procedure of ZnO NMs electrode and the corresponding supercapacitor. Figure 6b–d display the SEM images of the ZnO NMs with 50, 100, and 200 ALD cycles.

In different electrolytes, the ZnO NMs have different specific capacitance, 846 F g^{-1} (6 M KOH at 1 A g^{-1}), 465 F g^{-1} (1 M KCl at 1 A g^{-1}), and 65 F g^{-1} (6 M Na_2SO_4 at 1 A g^{-1}), respectively. However, those materials mentioned all have the problem of capacity attenuation during long-term cycling [135,136].

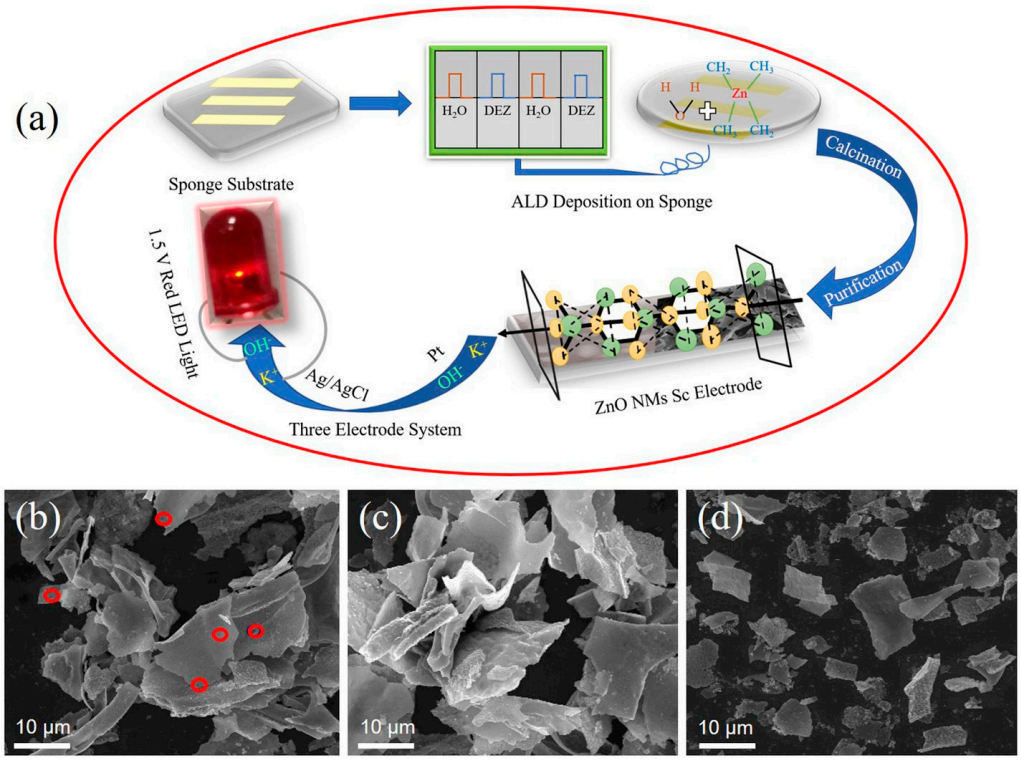

Figure 6. Design and morphologies of ZnO nanomembranes (NMs) with various thicknesses: (**a**) schematic of the fabrication procedure of ZnO NMs electrode and corresponding supercapacitor; (**b**–**d**) SEM images of ZnO NMs with (**b**) 50, (**c**) 100, and (**d**) 200 atomic layer deposition (ALD) cycles. The red circles in (**b**) represent the existence of the holes in ZnO NMs. Reproduced with permission from [134]. Copyright 2020 Elsevier.

2.4.1. ZnO-Based Composite Electrode

Numerous ZnO-based electrode materials are fabricated, such as carbon material-ZnO electrode [137–139], medal oxides-ZnO electrode [140–142], and polymer-ZnO electrode [143,144], for the purpose of pursuing good electrochemical performance. With asphalt as carbon source and ZnO as template, graphene nanocapsules (GNCs) [145] were synthesized by in situ KOH activation technology. High-speed channels for electron conduction, micropores for ion adsorption, and short pores for ion transport are provided by the 3D porous network. As supercapacitor electrodes, the GNCs exhibit great capacitance of 194 F g^{-1} at 20 A g^{-1} (277 F g^{-1} at 0.05 A g^{-1}) and capacitance loss of 2.6% after 15,000 cycles. Chebrolu et al. [146] fabricated a series of metal oxide composite nanostructures using the chemical bath deposition method. Those metal oxide composite nanostructures include ZnO nanowires, NiO nanosheets, ZnO/CuO nanowire arrays, ZnO/FeO nanocrystals, ZnO/NiO nanosheets, and ZnO/PbO nanotubes, among which ZnO/NiO nanosheets have the best electrochemical performance (at 8 mA cm^{-2} with a specific capacitance of 1248 F g^{-1} and long-term cycling stability). Because of ZnO/NiO nanosheets' unique surface morphology, increasing the electron transfer rate and electrical conductivity, the energy storage properties are improved. Di's group [147] reported that combing ZnO with a small amount of Al_2O_3 could prevent the ZnO nano-framework from collapsing. Meanwhile, the specific surface area of the material could be increased to enlarge the contact area between the composite and the electrolyte solution. The Al_2O_3-ZnO nanorod displays a high specific capacity (463.7 F g^{-1}) and favorable cyclic stability (96.9%), which is higher than Al_2O_3 and ZnO. In addition, the ion transferred number and the ion diffusion coefficient of the Al_2O_3-ZnO nanorod are 6.3 and 7.6 × 10^{-13} cm^2 s^{-1}. Studies have shown that the electrochemical properties can be further improved by synthesizing the ZnO-based multicomponent electrodes [65,148–150]. Obodo et al. [151] synthesized

Co_3O_4-CuO-ZnO@GO nanocomposite films by the hydrothermal method and then examined the effect of carbon ion irradiation on the properties of the prepared nanocomposite. The results of X-ray diffraction (XRD) suggest that low doses of carbon ion irradiation enhance the crystallinity of the materials, and high doses irradiation lead to deficiencies and disorder to the Co_3O_4-CuO-ZnO@GO, resulting in distortion and defects in the structure of the material. According to the study of electrochemical performance, the highest specific capacitance (1950 F g^{-1} at 10 mV s^{-1}) is obtained at a radiation dose of 5.0 × 10^{15} ions cm^{-2}, while the specific capacitance of 208 F g^{-1} and 1356 F g^{-1} are obtained at 1.0 × 10^{15} ions cm^{-2} and 7.0 × 10^{15} ions cm^{-2}, respectively. Self-assembled ZnO-CoO@nitrogen-doped carbon (NC) electrode [152] was prepared by the hydrothermal method combined with annealing. Owing to high conductivity, rich oxygen vacancies, and mesoporous structure, the electrode based on ZnO-CoO@NC shows a good cycle stability of 92% specific capacitance retention at 2 A g^{-1} (40,000 cycles) without morphology change. Besides, the graphene//ZnO-CoO@NC device also has 94% capacitance retention after 10,000 cycles at 2 A g^{-1}. At a potential window of 1.6 V, the device possesses an energy density of 16.5 W h kg^{-1} at a power density of 396.51 W kg^{-1} and remains at 5.5 W h kg^{-1} at 5634.5 W kg^{-1}.

2.4.2. Problems of ZnO-Based Electrode

A study [153] pointed out that the surface morphology of the powder coating became smoother and the exposed surface area lessened after a series of electrochemical reactions, because of which specific capacitance decreased. To solve this problem, ZnO rods are prepared by a hydrothermal method and then coated with a MoO_4^{2-} modified carbon layer (Mo-C) [154]. The carbon coating is composed of many tiny carbon spheres of 10–50 nm in size. Owing to the mesoporous structure, ZnO@Mo-C possesses a larger specific surface area (96.36 m^2 g^{-1}) than pure zinc oxide (0.835 m^2 g^{-1}). In addition, compared with the electrode material prepared by Mohamed's group [155], ZnO@Mo-C displays better capacitance and rate capability (900 F g^{-1} at 1 A g^{-1} and 650 F g^{-1} at 10 A g^{-1}). He and co-workers [156] constructed ZnO flower nanostructures on nickel foam coated with hierarchical α-$Co(OH)_2$. The unique structure increases the charge and ion transfer rates and improves the contribution of pseudoactive substances in faradaic reactions. An asymmetric supercapacitor is assembled in 3 M NaOH with NF@ZnO@$Co(OH)_2$ as positive electrode and NF@cellulose paper as the negative electrode. In cell voltage of 1.5 V, the asymmetric supercapacitor exhibits maximum energy density of 62.57 W h kg^{-1} at a power density of 71 1.28 W kg^{-1} and, at 16,985.55 W kg^{-1} (maximum power density), it delivers an energy density of 16.04 W h kg^{-1}. Ding et al. [157] anchored binder-free tin oxide nanosheets on nickel foam by a one-step hydrothermal method, and then CoS was deposited on the ZnO surface by electrodeposition. At a current density of 3 mA cm^{-2}, ZnO@CoS shows a high specific capacity of 898.9 C g^{-1}, while specific capacity of pristine ZnO and ZnO precursor are 614.4 C g^{-1} and 530.6 C g^{-1}, respectively. The assembled button-type asymmetric supercapacitor displays an energy density of 45.2 W h kg^{-1} at 1039.1 W kg^{-1} with an areal capacity of 2438 mC cm^{-2}. In addition, the capacity retention of 107% after 10,000 cycles shows its remarkable cycling stability. Table 1 shows the electrochemical performance of representative binary TMOs electrode materials.

Table 1. The electrochemical performance of representative binary transition metal oxides (TMOs) electrode materials. SWCNT, single-walled carbon nanotube; CVD, chemical vapor deposition.

Material	Preparation Method	Electrolyte	Specific Capacitance	Cycling Stability	Reference
RuO_2	hydrothermal method	1 M H_2SO_4	400 F g^{-1}	84.7% (6000 cycles)	[56]
MoS_2-RuO_2	hydrothermal method	1 M KOH	972 F g^{-1}	/	[59]
SWCNT/RuO_2/PIn	oxidation polymerization of indole	1 M H_2SO_4	1307 F g^{-1}	93% (3000 cycles)	[63]
reduced graphene oxide/Co_3O_4	hydrothermal method	2 M KOH	472 F g^{-1}	95.6% (1000 cycles)	[83]
Co_3O_4 nanowires	hydrothermal method	3 M KOH	310.4 C g^{-1}	80.3% (6000 cycles)	[87]
CeO_2/Co_3O_4/rGO nanoparticles	hydrothermal method	6 M KOH	1606.6 F g^{-1}	/	[92]
porous carbon/Co_3O_4	pyrolysis of precursor	3 M KOH	423 F g^{-1}	17% decay 2000 cycles	[100]
MnO_2 nanosheets/hollow carbon nanofibers	hydrothermal method	1 M Na_2SO_4	293.6 F g^{-1}	/	[104]
N-doped carbon@MnO_2	tannic acid-assisted etching process	1 M Na_2SO_4	247.9 F g^{-1}	82.9% (2000 cycles)	[117]
graphene/MnO_2 foam	CVD	1 M Na_2SO_4	333.4 F g^{-1}	92.2% (2000 cycles)	[123]
nitrogen-doped porous hollow carbon spheres/MnO_2	hydrothermal pre-carbonization and pyrolysis carbonization	1 M Na_2SO_4	255 F g^{-1}	89% (5000 cycles)	[125]
Zr-doped ZnO	physio-chemical	1 M KOH	518 F g^{-1}	94% (5000 cycles)	[133]
ZnO nanomembranes	atomic layer deposition	6 M KOH	846 F g^{-1}	89% (5000 cycles)	[134]
ZnO@rGO	direct microwave irradiation	0.1 M KOH	102.4 F g^{-1}	82.5% (3000 cycles)	[137]
Co_3O_4-CuO-ZnO/GO	hydrothermal method	0.5 M Na_2SO_4	2045 F g^{-1}	83.02% (5000 cycles)	[151]

2.5. XCo_2O_4 (X = Mn, Cu, Ni)

Ternary transition metal oxide XCo_2O_4 has a spinel structure. Generally, the two metal ions exhibit high capacity and conductivity, so ternary transition metal oxide has more abundant redox reactions and higher electrochemical activity than single metal oxides [158]. Thus, it has achieved great attention so far. When XCo_2O_4 is used as electrode material, the corresponding equations can be described as follows [52,159]:

$$MCo_2O_4 + H_2O + OH^- \leftrightarrow MOOH + 2CoOOH + e^- \quad (3)$$

$$2CoOOH + OH^- \leftrightarrow 2CoO_2 + H_2O + e^- \quad (4)$$

Shanmugavadivel and co-workers [160] prepared a $MnCo_2O_4$ electrode by a simple solution combustion method. At the scanning rate of 10 mV s^{-1}, the $MnCo_2O_4$ electrode shows the maximum specific capacitance of 270 F g^{-1}, and the capacitance attenuation after 1000 cycles is 7.6%. $MnCo_2O_4$ nanosheets [161] prepared by galvanostatic electrodeposition have the maximum specific capacitance of 585 F g^{-1} at 0.2 mA cm^{-2}. Furthermore, after 1500 cycles, the $MnCo_2O_4$ electrode possesses a capacity retention rate of 51.8%. A battery-type flexible electrode [162] was fabricated through coating mesoporous $NiCo_2O_4$ on an ultrafine nickel wire by electrodeposition, dealloying, and oxidation (Figure 7). The electrode is flexible and displays a high specific capacity of 315.4 C g^{-1} at 1 A g^{-1} and 8.4% area specific capacity loss after 50,000 cycles.

Via electrodeposition followed by air annealing, Pawar's group [54] synthesized ultrathin nanoporous $CuCo_2O_4$ nanosheets on a nickel foam. After 5000 cycles, $CuCo_2O_4$ nanosheets show the specific capacitance of 1473 F g^{-1} at 1 A g^{-1} with the capacity retention rate of 93%.

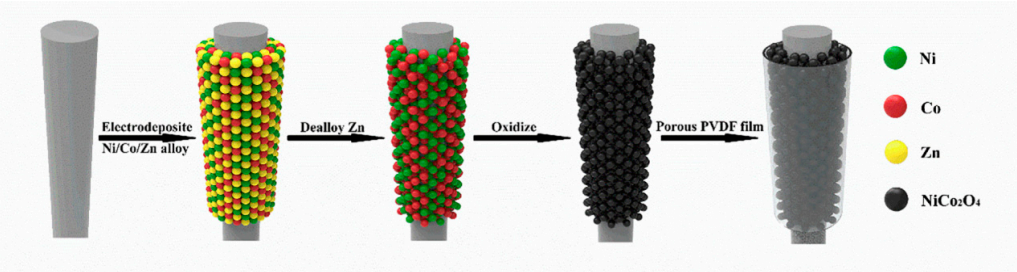

Figure 7. Schematic process showing the synthesis of porous polyvinylidene fluoride (PVDF)/$NiCo_2O_4$ coated on ultrafine nickel wire by electrodeposition and dealloying. Reproduced with permission from [162]. Copyright 2018 Elsevier.

2.5.1. Core–Shell Structure for MCo_2O_4-Based Electrode

The electrochemical performance of the MCo_2O_4-based electrodes above is not ideal and does not meet the requirements of high-performance supercapacitors. Because of the lack of active sites, serious agglomeration, and destruction of electrode materials during the long cycle, the electrochemical performance of the electrodes is weakened [55]. The core–shell structure has a large number of electroactive sites and fast ion diffusion. Moreover, ions and electrons are accessible to the interior of the electroactive materials. So, the composites in the core–shell structure can possess a good cycle life and rate retention. At the same time, compared with a single component, the heterostructure composites with two constituents deliver better electrochemical performances owing to the synergistic effect [127,148]. Therefore, researchers speculate that the proper design of the core–shell structure can improve the cycle stability and prevent the collapse during the cycle [163].

Wang's group [163] synthesized flower-like $MnCo_2O_4$ micro-nanostructures via a calcination process-assisted hydrothermal method. The prepared material possesses capacitance of 1933.33 F g^{-1} at 1 A g^{-1}. The $MnCo_2O_4$@$MnCo_2S_4$//CNTs device delivers brilliant cycle stability of 96% capacitance retention after 5000 cycles. At the same time, it shows high energy density of 50.75 Wh kg^{-1} at 1260 W kg^{-1}. Xu and co-workers [164] designed and prepared hierarchical mesoporous $NiCo_2O_4$@MnO_2 core–shell nanowire arrays on nickel foam. After 8000 cycles at 50 mA cm^{-2}, 113.6% original specific capacitance (1.23 F cm^{-2}) was obtained. An asymmetric supercapacitor was assembled with the prepared sample as the positive electrode and AC as the negative electrode. The measurement results show that, with the potential window of 1.5 V, the asymmetric supercapacitor delivers a specific capacitance of 112 F g^{-1} at 1 mA cm^{-2} and a maximum energy density of 35 W h kg^{-1}. In Zhu's study [165], the unique 3D hierarchical structure of $CuCo_2O_4$@$Ni(OH)_2$ provides large specific surface area, which enables rapid response and enhances electrochemical properties (2160 F g^{-1} at 1 A g^{-1} and a good capacitance retention of 82.7% at 20 A g^{-1}).

2.5.2. Introduction of Transition Metal Sulfides Materials

Transition metal sulfides have the characteristics of high faradic redox activities, unique physical or chemical properties, and long cycle performance. The conductivity of metal sulfides is higher than that of corresponding oxides, which is more convenient for electron transfer. In addition, low electroconductivity restricts TMOs further application in supercapacitors. At the same time, transition metal sulfides can make up for the shortcoming of TMOs. Moreover, because of the synergistic effect between the two individual materials, the mixed structure electrode can also improve the whole active region and promote the transport of ions from the electrolyte [19,166,167]. Liu and co-workers [167] fabricated Co_9S_8@$NiCo_2O_4$ nanobrushes by $NiCo_2O_4$ nanosheets grown on Co_9S_8 hollow nanoneedles. Owing to the good electrical conductivity and specific capacitance of Co_9S_8 and large specific surface area provided by the hollow nanoneedles structure, remarkable electrochemical properties are displayed (a high specific capacitance of 1966 F g^{-1} at 1 A g^{-1} and excellent capacitance retention of 92.9% after 5000 cycles).

Owing to its unique structure, $CuCo_2S_4/CuCo_2O_4$ has the advantages of electrochemical surface area, excellent conductivity, short ion diffusion path, and rapid electron and ion transport rate [168]. Based on graphene aerogel and $CuCo_2S_4/CuCo_2O_4$, the asymmetric supercapacitor is synthesized, which delivers energy density of 33.2 W h kg^{-1}, power density of 13.3 kW kg^{-1}, and outstanding long-term stability of 73% capacitance retention after 10,000 cycles.

2.5.3. Introduction of Oxygen Vacancies

There are three reasons that can explain why the introduction of oxygen vacancies is an effective strategy to improve the electrochemical performance. (i) Introduction of oxygen vacancies can adjust the surface chemical structure and enlarge the electroactive sur-face area exposed to the electrolyte. (ii) Oxygen vacancies can help the diffusion for charge carriers. Therefore, the conductivity of TMOs is improved. (iii) Electrochemical active sites are created when oxygen vacancies are introduced because the oxygen vacancies can serve as active sites for redox reactions. The kinetics of surface reactions is accelerated and the capacitance is increased [169–171]. To improve slow reaction kinetics and poor conductivity of $CuCo_2O_4$ electrode material, Feng et al. [170] prepared oxygen-vacancy-enriched $CuCo_2O_4$ nanoflowers in hypoxic atmosphere via a hydrothermal method followed by thermal treatment. The presence of oxygen defect sites and impurity bands provides massive reaction sites and fast ion intercalation, which improves electrical conductivity and hydrophilic properties. The electrode material shows a brilliant specific capacitance of 1.2 F cm^{-2} at 1.2 mA cm^{-2} and rate capability of 69.4% capacitance retention at 20 A g^{-1}. Yan et al. [171] soaked the prepared $NiCo_2O_4$ nanostructures in the different concentration of $NaBH_4$ solution (0.1 M, 0.3 M, 0.5 M, 0.7 M) to change the content of oxygen vacancies (Figure 8).

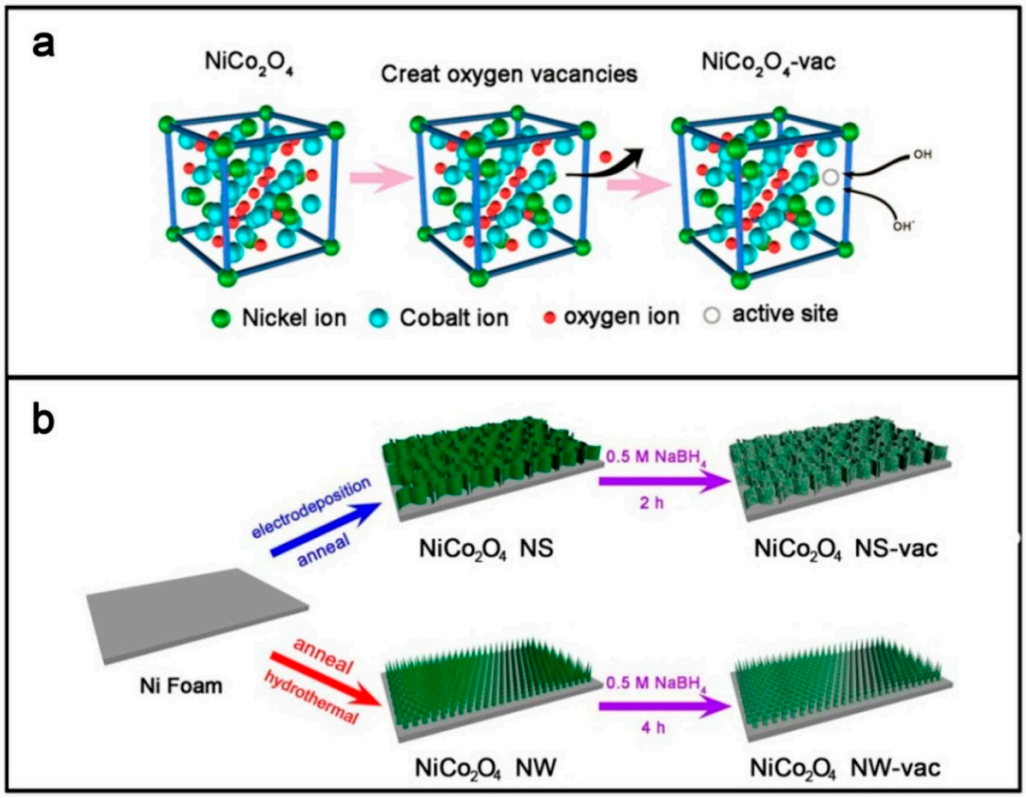

Figure 8. (**a**) Schematic diagram of oxygen vacancies in $NiCo_2O_4$; (**b**) the preparation scheme of the electrodes. Reproduced with permission from [171]. Copyright 2018 Elsevier.

The results indicate that an appropriate oxygen vacancy content can increase the diffusion rate of carriers. In addition, oxygen vacancies as active sites for redox reactions can accelerate the surface kinetics reaction. The $NiCo_2O_4$ nanosheets electrode treated with 0.5 M $NaBH_4$ has the best electrochemical performance (1590 F g^{-1} at 1 A g^{-1} and a capacitance retention of 79.12% at 10 A g^{-1} after 10,000 cycles).

2.6. $AMoO_4$ (A = Co, Mn, Ni, Zn)

Compared with carbon materials, pseudocapacitive materials like metal oxides and organic conductive materials have higher specific capacitance owing to redox reaction on the surface of the material. In addition, ternary metal oxides have more active sites and faster redox reactions than single metal oxides, which become one of the materials to replace RuO_2 [53,172–174]. As the hotspots of mixed transition metal oxides, the transition metal molybdates have attracted much attention because of their advantages including natural abundance, high theoretical specific capacitance, and low costs [175]. The performance of supercapacitors depends largely on the morphology and structure of their electrode materials. Therefore, it is very important to design electrode materials with unique spatial structure characteristics [176].

2.6.1. Core–Shell Structure for $AMoO_4$-Based Electrode

According to Yi's study [127], the design of heterostructure composites has proved to be a hopeful way to promote the electrochemical properties of TMOs. Core–shell structure is a kind of heterostructure. The core–shell structure can supply large specific surface area with rich porosity. Meanwhile, the electron transfer rate is accelerated by core materials and electrochemical redox active sites are provided by shell materials. The volume changes during the cycle process are adjusted by the structure. In addition, the synergistic effect of each component is utilized to improve the electrochemical performance of the electrode [177–180]. Xuan et al. [181] designed and prepared 3D self-supported hierarchical $CoMoO_4$@CoS core–shell heterostructures on rGO/Ni foam. Figure 9 shows the SEM images of $CoMoO_4$, CoS, and $CoMoO_4$@CoS with different magnification.

The unique material structure, the excellent conductivity of rGO, and the synergistic effect between the two materials help to increase the electrochemical active sites and enhance the capacitance. According to the electrochemical performance tests, the core–shell $CoMoO_4$@CoS composite shows 81.1% retention of the initial capacitance (3380.3 F g^{-1} at 1 A g^{-1}) after 6000 cycles at 10 A g^{-1}. In order to further improve the performance of MCo_2O_4 materials, Hussain and co-workers [182] combined $CoMoO_4$ with ternary metal sulfide $NiCo_2S_4$ to synthesize three-dimensional walking palm-like core–shell $CoMoO_4$@$NiCo_2S_4$@NF nanostructure by a two-step hydrothermal method. At a current density of 5 mA cm^{-2}, the synthesized composite exhibits a high capacitance of 17.0 F cm^{-2}. Besides, 114% capacitance retention after 10,000 charge/discharge cycles reveals its remarkable cycling stability. The asymmetric supercapacitor fabricated with $CoMoO_4$@$NiCo_2S_4$@NF and AC@NF as electrodes shows a high energy density of 60.2 W h kg^{-1} at a power density of 188 W kg^{-1}. Moreover, it lights 22 parallel-connected red light emitting diodes for over 60 s.

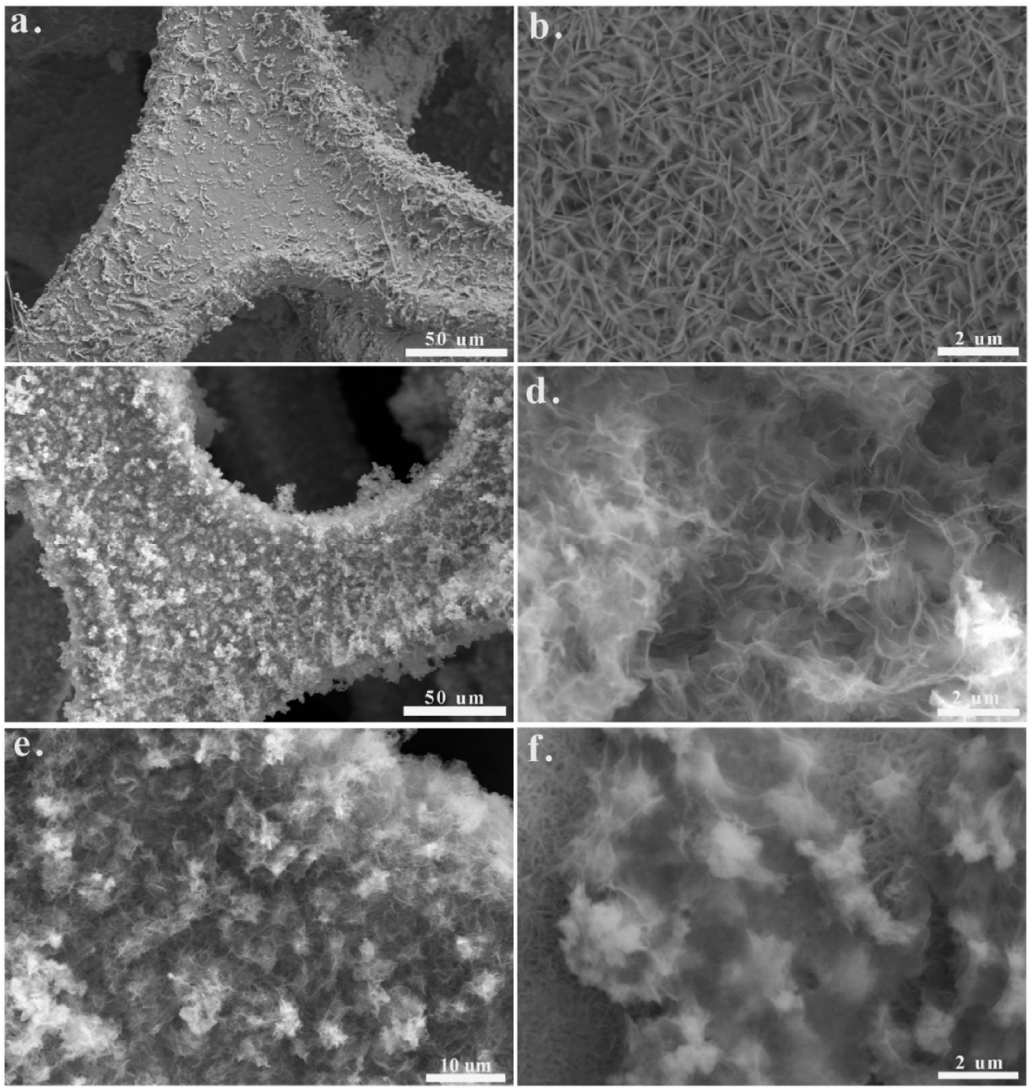

Figure 9. (**a**,**b**) SEM images of $CoMoO_4$ with different magnification; (**c**,**d**) SEM images of CoS with different magnification; (**e**,**f**) SEM images of $CoMoO_4$@CoS with different magnification. Reproduced with permission from [181]. Copyright 2020 Elsevier.

2.6.2. Modification of Quantum Dots

Quantum dots (QDs) are zero-dimensional nanoparticles of metal or semiconductor crystals with a diameter between 2 and 8 nanometers [183]. Quantum dots have attracted much attention for various applications owing to their characteristics such as quantum tunneling effect, surface effect, and quantum confinement effect [184]. It is noteworthy that the size of the material largely decides the substantial variation of fundamental electrical and optical properties [185]. Therefore, optical, electronic, and mechanical properties of QDs are different from corresponding nanoparticles [186]. For example, infinite exciton Bohr radius converts graphene to graphene quantum dots (GQDs) and GQDs start to fluoresce because electron distribution is transparently modified by the crystal boundary with the dimension of the crystal reducing to a nanometer scale [185]. Moreover, some unique properties of zero-dimensional nanoparticles like distinct edge and quantum confinement effects help to improve the electrochemical performance [183]. Some studies prove that quantum dot modification is an effective method for improving electrochemical performance [187–189]. Hence, it can be speculated that quantum dot modification is a promising strategy to improve the performance of $AMoO_4$-based electrode. To the best of our knowledge, there are still relatively few reports in this regard. Zhu et al. [190]

synthesized carbon quantum dots (CQDs) modified porous $NiCo_2O_4$ sphere composites. The CQDs/$NiCo_2O_4$ composite electrode possesses a specific capacitance (856 F g^{-1} at 1 A g^{-1}) and excellent rate capability of 83.9%, 72.5%, and 60.8% capacity retention rate at 20, 50, and 100 A g^{-1}, respectively. It also has 1.25% capacitance loss over 10,000 cycles at 5 A g^{-1}, which indicates its exceptional cycling stability. The maximum capacitance of graphene quantum dot modified nano-needle electrode [191] at 1 A g^{-1} is four times higher than that of pure $MnCo_2O_{4.5}$ nano-spherical electrode (1625 F g^{-1} and 368 F g^{-1}, respectively). In Zhang's research [192], mesoporous $NiMoO_4$ microspheres were modified by silver quantum dots to fabricate the Ag QDs/$NiMoO_4$ microspheres (Figure 10).

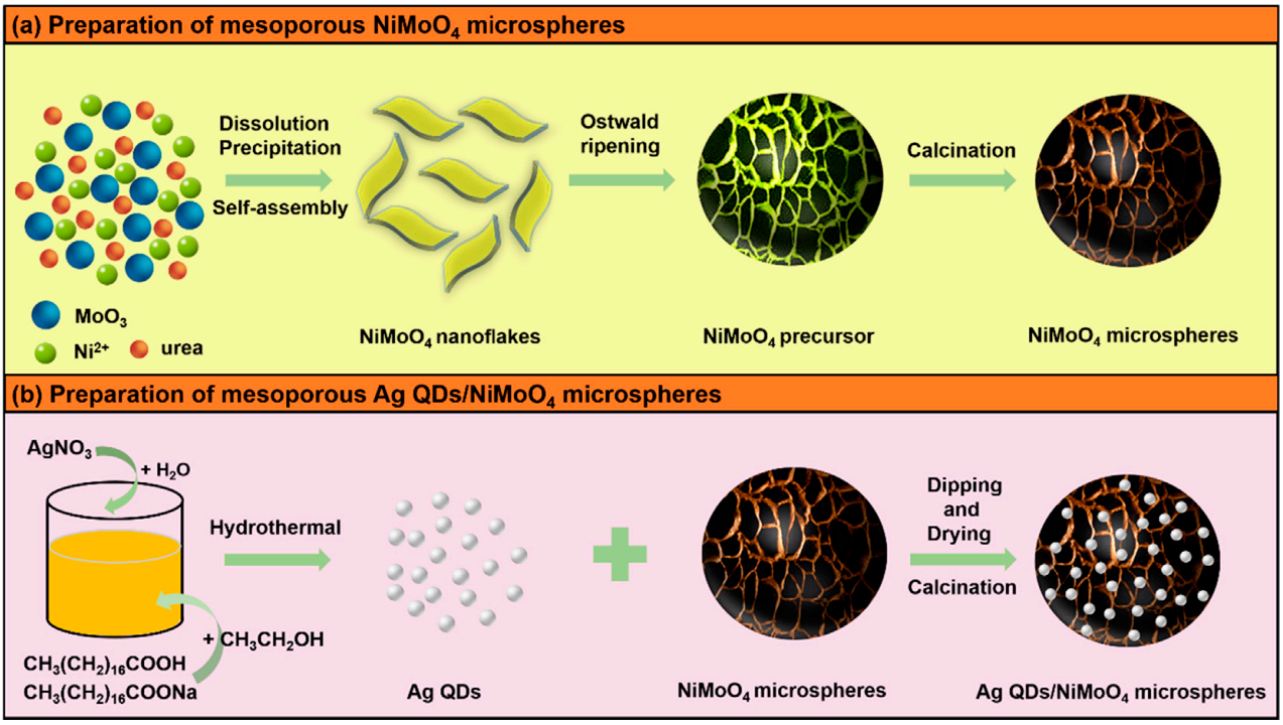

Figure 10. (**a**) Schematic illustration of the synthesis processes for mesoporous $NiMoO_4$ microspheres; (**b**) schematic illustration of the synthesis processes for Ag quantum dots (QDs)/$NiMoO_4$ microspheres. Reproduced with permission from [192]. Copyright 2020 Elsevier.

Owing to high specific surface area, plenty of active sites, enhanced interfacial conductivity, and porous structure, the Ag QDs/$NiMoO_4$ microspheres exhibit specific capacitance of 3342.7 F g^{-1} at 1 mV s^{-1} and 2074 F g^{-1} at 1 A g^{-1} (Figure 11).

Moreover, the asymmetric supercapacitor assembled with Ag QDs/$NiMoO_4$ and spore-derived activated carbon delivers high energy density of 48.5 W h kg^{-1} at a power density of 212.5 kW h kg^{-1} and good cycling performance. Table 2 shows the performance of representative electrodes based binary and ternary TMOs, and Table 3 shows the performance of representative supercapacitors based on binary and ternary TMOs.

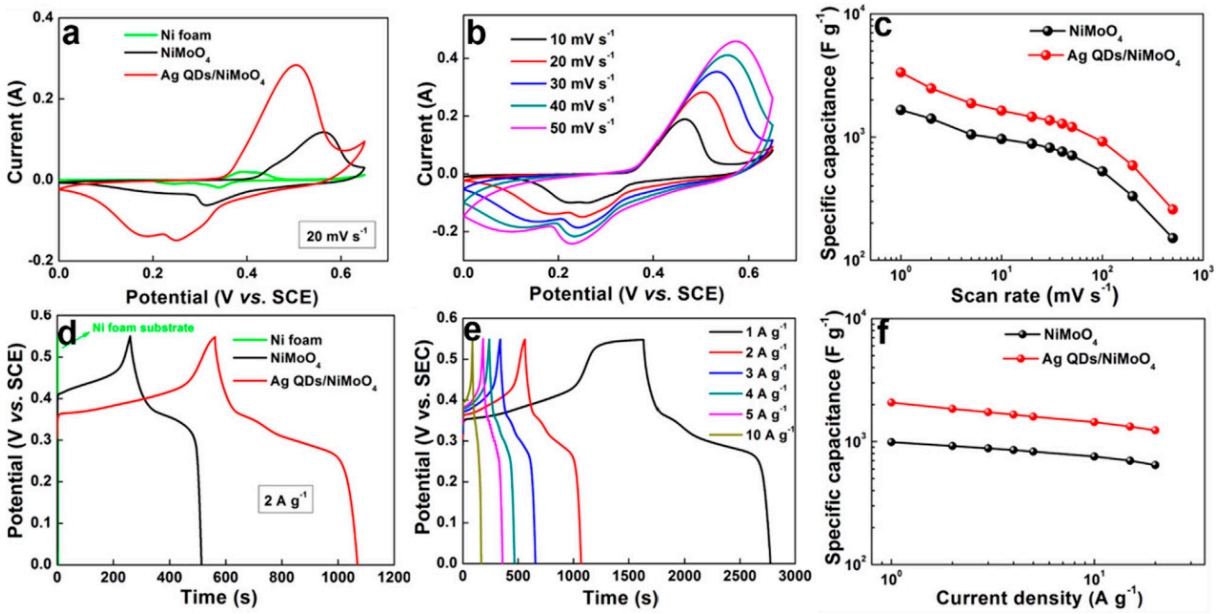

Figure 11. CV and GCD measurements for the $NiMoO_4$ and Ag QDs/$NiMoO_4$ electrodes in the three-electrode system: (**a**) contrastive CV curves at 20 mV s^{-1}; (**b**) CV curves of Ag QDs/$NiMoO_4$ electrode; (**c**) specific capacitances as a function of scan rates; (**d**) contrastive GCD curves at 2 A g^{-1}; (**e**) rate performances of Ag QDs/$NiMoO_4$ electrode; and (**f**) specific capacitances as a function of current densities. Reproduced with permission from [192]. Copyright 2020 Elsevier.

Table 2. The performance of electrodes based on binary and ternary TMOs.

Category	Electrode Material	Electrolyte	Specific Capacitance	Cycling Stability	Reference
binary transmission metal oxides	$CuCo_2O_4$/CuO@RuO_2	2 M KOH	862.5 mAh cm^{-2}	90.1% (8000 cycles)	[64]
	NiO/Co_3O_4	3 M KOH	1242 C g^{-1}	95.5% (12,000 cycles)	[75]
	Co_3O_4 micro-bundles	2 M KOH	282.3 C g^{-1}	74.6% (4000 cycles)	[51]
	Ag-doped Co_3O_4/NF	3 M KOH	1425 F g^{-1}	96.4 (5000 cycles)	[91]
	Co_3O_4@MnO_2 on carbon cloth	1 M Na_2SO_4	616.7 F g^{-1}	83.1% (10,000 cycles)	[128]
	NiO@MnO_2	/	1219.2 F g^{-1}	76.7% (10,000 cycles)	[127]
	ZnO/CeO_2	0.2 M K4(Fe[CN]$_6$) in 3 M KOH	495.4 F g^{-1}	95.6% (2000 cycles)	[140]
	ZnO@Mo–C	2 M KOH	900 F g^{-1}	/	[154]
	graphene quantum dots/$MnCo_2O_{4.5}$	2M KOH	1625 F g^{-1}	80% (5000 cycles)	[191]
ternary transmission metal oxides	Ag QDs/$NiMoO_4$	3 M KOH	2074 F g^{-1}	81% (1000 cycles)	[192]
	$CoMoO_4$@$NiCo_2S_4$@Nickel Foam	3 M KOH	17.0 F cm^{-2}	114% 10,000 cycles.	[182]
	$CuCo_2O_4$@$Ni(OH)_2$	2 M KOH	2160 F g^{-1}	92% (5000 cycles)	[165]
	Co_9S_8@$NiCo_2O_4$	3 M KOH	1966 F g^{-1}	92.9% (5000 cycles)	[167]
	$CoMoO_4$@$MoZn_{22}$	3 M KOH	923 C g^{-1}	92.3% (7000 cycles)	[177]

Table 3. The performance of supercapacitors based on binary and ternary TMOs.

Electrode Material	Operating Voltage	Specific Capacitance	Energy Density	Cycling Stability	Reference
RuO_2//h-WO_3	1.6 V	47.59 F g^{-1}	16.92 W h kg^{-1}	~171.75% (6500 cycles)	[72]
Co_3O_4//AC	1.6 V	310.4 C g^{-1}	0.4 mW h cm^{-3}	79.2% (10,000 cycles)	[87]
Co_3O_4-NiO/GO//AC	1.65 V	133 F g^{-1}	50.2 W h kg^{-1}	82% (3000 cycles)	[91]
Co_3O_4/NF—8 h//N-rGO/NF	1.6 V	62.5 F g^{-1}	22.2 W h kg^{-1}	93.3% (10,000 cycles)	[93]
MnO_2/HCS-30//HCS	2.0 V	74.5 F g^{-1}	41.4 W h kg^{-1}	93.9% (5000 cycles)	[125]
Co_3O_4@MnO_2@CC-90//AC	2.2 V	309.2 mF cm^{-2}	54.71 W h kg^{-1}	86.3% (10,000 cycles)	[128]
graphene electrode//ZnO-CoO@NC	1.6 V	/	16.5 W h kg^{-1}	about 94% (10,000 cycles)	[152]
ZnO@CoS//AC	1.6 V	2438 mC cm^{-2}	45.2 W h kg^{-1}	107% (11,000 cycles)	[157]
$NiCo_2O_4$@MnO_2//AC	1.5 V	112 F g^{-1}	35 W h kg^{-1}	~71% (5000 cycles)	[164]
$CuCo_2S_4$/$CuCo_2O_4$//graphene aerogel	1.6 V	90.4 F g^{-1}	33.2 W h kg^{-1}	73% (10,000 cycles)	[168]
$CoMoO_4$@CoS//AC	1.7 V	189.5 F g^{-1}	59.2 W h kg^{-1}	91.5% (6000 cycles)	[181]
$CoMoO_4$@$NiCo_2S_4$@NF//AC@NF	1.6 V	182 F g^{-1}	60.2 W h kg^{-1}	84% (5000 cycles)	[182]
$MnCo_2O_{4.5}$-40 GQDs//rGO	1.3 V	200 F g^{-1}	46 W h kg^{-1}	77% (5000 cycles)	[191]
Ag QDs/ $NiMoO_4$//spore-derived AC	1.7 V	120.5 F g^{-1}	48.5 W h kg^{-1}	84.4% (5000 cycles)	[192]

3. Conclusions

The main purpose of developing supercapacitors is to meet the requirement of storing renewable energy. Supercapacitors have the advantages of high-power density, excellent cycle stability, and fast charge/discharge process. The performance of supercapacitors largely depends on the electrode materials. TMOs are the most favored because of their higher energy density and specific capacity than carbon materials, and better chemical stability than conductive polymers.

In this review, we have summarized recent developments of TMOs-based electrode materials for supercapacitors, including design, fabrication, and electrochemical performances. RuO_2 is the ideal TMOs electrode material, but high cost and toxicity are its fatal shortcomings. Co_3O_4, MnO_2, and ZnO are supposed to substitute RuO_2. However, existing problems like low conductivity hinder their practical application in electrode materials. Therefore, we have introduced some strategies to solve the problems. (i) Preparing nano scale materials. The small size enlarges the contact surface and shortens the ion diffusion distance between materials and electrolyte. The size of material largely decides the substantial variation of fundamental electrical and optical properties. In addition, optical, electronic, and mechanical properties of QDs are different from corresponding nanoparticles. That is why QDs are very attractive in various fields. (ii) Utilizing the synergistic effect. It is very important that, through different combinations of carbon materials, transition metal oxides, transition metal sulfides, and other materials, the synergistic effect between different components can be used to improve the electrochemical performance effectively. In addition, some electrode materials containing metal sulfides exhibit good electrochemical performance, which indicates that other binary metal materials such as metal phosphides and metal nitrides also have potential for electrode materials. (iii) Synthesizing composites with a special structure. Porous structure, core–shell structure, and hollow structure can enlarge the surface area with generous electrochemical active sites and reduce the resistance of ion and electron transfer, thus increasing the conductivity and the rate of redox reaction. Further, the introduction of oxygen vacancies can not only increase active sites, but also adjust the surface chemical structure, improving the conductivity. (iv) Ternary transition oxides have higher conductivity, faster faradic reaction, and more active sites than single metal oxides. At the same time, Tables 1–3 show that ternary transition oxides have better performance than single transition oxides in the practical application of both electrode and supercapacitor. We believe that ternary TMOs will be the focus of future research on transition metal oxides.

Although much promising progress has been obtained in TMOs-based electrode materials, low energy density is still an obstacle for the development of supercapacitors. We have three recommendations on the development of supercapacitors. (i) Researchers should aim efforts towards how to obtain raw material of electrode with low cost and no pollution, and the use of biomass carbon materials is a good example. (ii) The development of portable and wearable electronic devices drives the study of flexible supercapacitors. That means, apart from increasing the energy density, it is necessary to achieve the stability of the capacitance performance under different bending and deformation conditions. (iii) At present, there are many reports on transparent and flexible electrodes for solar batteries. Moreover, supercapacitors based on battery-type electrodes are also widely reported. At the same time, hybrid supercapacitors can shorten the gap between conventional metal ion batteries and supercapacitors [52]. We wonder whether supercapacitors could have the possibility of solar charging in the future. If the wonder come true, that will represent significant progress in the development of supercapacitors.

Author Contributions: Conceptualization, R.L., Y.D. and P.X.; investigation, J.C. (Junyang Cheng), S.Y. and Y.C.; data curation, J.C.; writing—original draft preparation, R.L.; writing—review and editing, R.L., Y.D. and P.X.; supervision, J.C. (Jianwen Chen) and J.Y. All authors have read and agreed to the published version of the manuscript.

Funding: This work was supported by National Natural Science Foundation of China (Grant No. 61804029), Research Fund of Guangdong-Hong Kong-Macao Joint Laboratory for Intelligent Micro-Nano Optoelectronic Technology (No. 2020B1212030010), Guangdong Provincial Key Laboratory of Semiconductor Micro Display (2020B121202003), and the Project of Foshan Education Bureau (Grant No. 2019XJZZ02).

Conflicts of Interest: The authors declare no conflict of interest.

References

1. Liu, P.Y.; Zhao, J.J.; Dong, Z.P.; Liu, Z.L.; Wang, Y.Q. Interwoving Polyaniline and a Metal-organic Framework Grown in Situ for Enhanced Supercapacitor Behavior. *J. Alloys Compd.* **2021**, *854*, 157181.
2. Prakash, D.; Manivannan, S. Unusual Battery Type Pseudocapacitive Behaviour of Graphene Oxynitride Electrode: High Energy Solid-state Asymmetric Supercapacitor. *J. Alloys Compd.* **2021**, *854*, 156853. [CrossRef]
3. Sethi, M.; Shenoy, U.S.; Bhat, D.K. Simple Solvothermal Synthesis of Porous Graphene-NiO Nanocomposites with High Cyclic Stability for Supercapacitor Application. *J. Alloys Compd.* **2021**, *854*, 157190. [CrossRef]
4. Sun, Z.Q.; Li, F.Z.; Ma, Z.Q.; Wang, Q.; Qu, F.Y. Battery-type Phosphorus Doped FeS_2 Grown on Graphene as Anode for Hybrid Supercapacitor with Enhanced Specific capacity. *J. Alloys Compd.* **2021**, *854*, 157114. [CrossRef]
5. Wang, Y.; Qiao, M.F.; Mamat, X. Nitrogen-doped Macro-meso-micro Hierarchical Ordered Porous Carbon Derived from ZIF-8 for Boosting Supercapacitor Performance. *Appl. Surf. Sci.* **2021**, *540*, 148352.
6. Zan, G.T.; Wu, T.; Chen, H.X.; Dong, F.Q.; Wu, Q.S. $BiVO_4$ Nanocoral Superstructures and Their Excellent Electrical/optical Dual-functions. *J. Alloys Compd.* **2021**, *852*, 157035.
7. Wu, S.R.; Liu, J.B.; Wang, H.; Yan, H. A Review of Performance Optimization of MOF-derived Metal Oxide as Electrode Materials for Supercapacitors. *Int. J. Energy Res.* **2019**, *43*, 697–716.
8. Anand, S.; Ahmad, M.W.; Al Saidi, A.K.A.; Yang, D.-J.; Choudhury, A. Polyaniline Nanofiber Decorated Carbon Nanofiber Hybrid Mat for Flexible Electrochemical Supercapacitor. *Mater. Chem. Phys.* **2020**, *254*, 123480. [CrossRef]
9. Hu, Q.L.; Yue, B.; Shao, H.Y.; Yang, F.; Wang, J.H.; Wang, Y.; Liu, J.H. Facile Syntheses of Perovskite Type $LaMO_3$ (M = Fe, Co, Ni) Nanofibers for High Performance Supercapacitor Electrodes and Lithium-ion Battery Anodes. *J. Alloys Compd.* **2021**, *852*, 157002.
10. Kumar, K.S.; Choudhary, N.; Pandey, D.; Hurtado, L.; Chung, H.-S.; Tetard, L.; Jung, Y.W.; Tomas, J. High-performance Flexible Asymmetric Supercapacitor Based on rGO Anode and WO_3/WS_2 Core/shell Nanowire Cathode. *Nanotechnology* **2020**, *31*, 435405. [CrossRef] [PubMed]
11. Yu, J.H.; Gao, X.L.; Cui, Z.X.; Jiao, Y.; Zhang, Q.; Yu, L.Y.; Dong, L.Y. Facile Synthesis of Binary Transition Metal Sulfide Tubes Derived from NiCo-MOF-74 for High-performance Supercapacitors. *Energy Technol.* **2019**, *7*, 1900018.
12. Shin, S.Y.; Shin, M.W. Nickel Metal–organic Framework (Ni-MOF) Derived NiO/C@CNF Composite for the Application of High Performance Self-standing Supercapacitor Electrode. *Appl. Surf. Sci.* **2021**, *540*, 148295.
13. Liu, Y.M.; Murtaza, I.; Shuja, A.; Meng, H. Interfacial Modification for Heightening the Interaction between PEDOT and Substrate Towards Enhanced Flexible Solid Supercapacitor Performance. *Chem. Eng. J.* **2020**, *379*, 122326.
14. Gao, Y.-P.; Zhai, Z.-B.; Wang, Q.-Q.; Hou, Z.-Q.; Huang, K.-J. Cycling Profile of Layered $MgAl_2O_4$/reduced graphene oxide Composite for Asymmetrical Supercapacitor. *J. Colloid Interface Sci.* **2019**, *539*, 38–44.

15. Meng, Z.H.; Yan, W.; Zou, M.Y.; Miao, H.; Ma, F.X.; Patil, A.B.; Yu, R.; Liu, X.Y.; Liu, N.B. Tailoring NiCoAl Layered Double Hydroxide Nanosheets for Assembly of High-performance Asymmetric Supercapacitors. *J. Colloid Interface Sci.* **2021**, *583*, 722–733.
16. Gao, Y.-P.; Huang, K.-J. $NiCo_2S_4$ Materials for Supercapacitor Applications. *Chem. Asian J.* **2017**, *12*, 1969–1984.
17. Du, Y.Q.; Xiao, P.; Yuan, J.; Chen, J.W. Research Progress of Graphene-Based Materials on Flexible Supercapacitors. *Coatings* **2020**, *10*, 892.
18. Chameh, B.; Moradi, M.; Hajati, S.; Hessari, F.A. Design and Construction of ZIF (8 and 67) Supported Fe_3O_4 Composite as Advanced Materials of High Performance Supercapacitor. *Phys. E Syst. Nanostruct.* **2021**, *126*, 114442. [CrossRef]
19. Niu, W.S.; Xiao, Z.Y.; Wang, S.F.; Zhai, S.R.; Qin, L.F.; Zhao, Z.Y.; An, Q.D. Synthesis of Nickel Sulfide-supported on Porous Carbon from a Natural Seaweed-derived Polysaccharide for High-performance Supercapacitors. *J. Alloys Compd.* **2021**, *853*, 157123.
20. Pettong, T.; Iamprasertkun, P.; Krittayavathananon, A.; Sukha, P.; Sirisinudomkit, P.; Seubsai, A.; Chareonpanich, M.; Kongkachuichay, P.; Limtrakul, J.; Sawangphruk, M. High-performance Asymmetric Supercapacitors of $MnCo_2O_4$ Nanofibers and N-doped Reduced Graphene Oxide Aerogel. *ACS Appl. Mater. Inter.* **2016**, *8*, 34045–34053. [CrossRef]
21. Zhou, W.; Han, G.Y.; Xiao, Y.M.; Chang, Y.Z.; Yuan, W.; Li, Y.P.; Liu, C.X.; Zhang, Y. Polypyrrole Doped with Dodecyl Benzene Sulfonate Electrodeposited on Carbon Fibers for Flexible Capacitors with High-performance. *Electrochim. Acta* **2015**, *176*, 594–603.
22. Sun, L.; Fu, Q.; Pan, C.X. Mn_3O_4 Embedded 3D Multi-heteroatom Codoped Carbon Sheets/carbon Foams Composites for High-performance Flexible Supercapacitors. *J. Alloys Compd.* **2020**, *849*, 156666.
23. Liu, S.L.; Feng, Q.C.; Zhang, C.; Liu, T.X. Molten Salt-confined Pyrolysis towards Carbon Nanotube-backboned Microporous Carbon for High-energy-density and Durable Supercapacitor Electrodes. *Nanotechnology* **2021**, *32*, 095605.
24. Zhang, M.M.; Song, Z.X.; Liu, H.; Wang, A.; Shao, S.Y. MoO_2 Coated Few Layers of MoS_2 and FeS_2 Nanoflower Decorated S-doped Graphene Interoverlapped Network for High-energy Asymmetric Supercapacitor. *J. Colloid Interface Sci.* **2021**, *584*, 418–428. [CrossRef]
25. Wu, P.; Cheng, S.; Yao, M.H.; Yang, L.F. A low-cost, Self-standing $NiCo_2O_4$@CNT/CNT Multilayer Electrode for Flexible Asymmetric Solid-state Supercapacitors. *Adv. Funct. Mater.* **2017**, *27*, 1702160.
26. Liu, Y.B.; Huang, G.X.; Li, Y.Y.; Yao, Y.H.; Xing, B.L.; Liu, Q.R.; Jia, J.B.; Zhang, C.X. Structural Evolution of Porous Graphitic Carbon Nanosheets Based on Quinonyl Decomposition for Supercapacitor Electrodes. *Appl. Surf. Sci.* **2021**, *537*, 147824.
27. Shi, Y.; Sun, L.; Zhang, Y.X.; Si, H.C.; Sun, C.; Gu, J.L.; Gong, Y.; Li, X.W.; Zhang, Y.H. SnS_2 Nanodots Decorated on RGO Sheets with Enhanced Pseudocapacitive Performance for Asymmetric Supercapacitors. *J. Alloys Compd.* **2021**, *853*, 156903.
28. Hao, J.Y.; Zou, X.F.; Feng, L.; Li, W.P.; Xiang, B.; Hu, Q.; Liang, X.Y.; Wu, Q.B. Facile Fabrication of Core-shell Structured $Ni(OH)_2/Ni(PO_3)_2$ Composite via One-step Electrodeposition for High Performance Asymmetric Supercapacitor. *J. Colloid Interface Sci.* **2021**, *583*, 243–254.
29. Zhai, S.X.; Jin, K.; Zhou, M.; Fan, Z.Z.; Zhao, H.; Li, X.Y.; Zhao, Y.P.; Ge, F.Y.; Cai, Z.S. A Novel High Performance Flexible Supercapacitor Based on Porous Carbonized cotton/ZnO Nanoparticle/CuS Micro-sphere. *Colloids Surf. A* **2020**, *584*, 124025.
30. He, W.D.; Wang, C.G.; Zhuge, F.W.; Deng, X.L.; Xu, X.J.; Zhai, T.Y. Flexible and High Energy Density Asymmetrical Supercapacitors Based on Core/shell Conducting Polymer Nanowires/manganese Dioxide Nanoflakes. *Nano Energy* **2017**, *35*, 242–250.
31. Liu, B.G.; Shi, R.; Chen, R.F.; Wang, C.H.; Zhou, K.; Ren, Y.D.; Zeng, Z.; Liu, Y.Y.; Li, L.Q. Optimized Synthesis of Nitrogen-doped Carbon with Extremely High Surface Area for Adsorption and Supercapacitor. *Appl. Surf. Sci.* **2021**, *538*, 147961.
32. Padya, B.; Kali, R.; Enaganti, P.K.; Narasaiah, N.; Jain, P.K. Facile Synthesis and Frequency-response Behavior of Supercapacitor Electrode Based on Surface-etched Nanoscaled-graphene Platelets. *Colloid. Surf. A* **2021**, *609*, 125587. [CrossRef]
33. Avasthi, P.; Arya, N.; Singh, M.; Balakrishnan, V. Fabrication of iron Oxide-CNT Based Flexible Asymmetric Solid State Supercapacitor Device with High Cyclic Stability. *Nanotechnology* **2020**, *31*, 435402. [CrossRef] [PubMed]
34. Zhang, Y.; Zhang, L.; Cheng, L.; Yang, D.D.; Wan, L.; Chen, J.; Xie, M.J. Synthesis of Faradaic-active N,O-doped Carbon Nanosheets from M-trihydroxybenzene and Piperazine for High-performance Supercapacitor. *Appl. Surf. Sci.* **2021**, *538*, 148040. [CrossRef]
35. Yang, G.J.; Park, S.J. MnO_2 and Biomass-derived 3D Porous Carbon Composites Electrodes for High Performance Supercapacitor Applications. *J. Alloys Compd.* **2018**, *741*, 360–367.
36. Li, C.J.; Dong, X.Q.; Zhang, Y.C.; Hu, J.; Liu, W.W.; Cui, X.; Hao, A.Y. MnO_x Nanosheets Anchored on a Bio-derived Porous Carbon Framework for High-performance Asymmetric Supercapacitors. *Appl. Surf. Sci.* **2020**, *527*, 146842.
37. Chen, H.; Li, W.L.; He, M.; Chang, X.W.; Zheng, X.L.; Ren, Z.Y. Vertically Oriented Carbon Nanotube as a Stable Frame to Support the $Co_{0.85}Se$ Nanoparticles for High Performance Supercapacitor Electrode. *J. Alloys Compd.* **2021**, *855*, 157506.
38. Wang, N.; Zhao, P.; Liang, K.; Yao, M.Q.; Yang, Y.; Hu, W.C. CVD-grown Polypyrrole Nanofilms on Highly Mesoporous Structure MnO_2 for High Performance Asymmetric Supercapacitors. *Chem. Eng. J.* **2017**, *307*, 105–112.
39. Kuo, C.-W.; Chang, J.-C.; Wu, B.-W.; Wu, T.-Y. Electrochemical Characterization of RuO_2-Ta_2O_5/polyaniline Composites as Potential Redox Electrodes for Supercapacitors and Hydrogen Evolution Reaction. *Int. J. Hydrogen Energy* **2020**, *45*, 22223–22231.
40. Ates, M.; Yildirim, M. The Synthesis of rGO/RuO_2, rGO/PANI, RuO_2/PANI and rGO/RuO_2/PANI Nanocomposites and Their Supercapacitors. *Polym. Bull.* **2020**, *77*, 2285–2307.
41. Wang, G.R.; Jin, Z.L.; Guo, Q.J. Ordered Self-supporting NiV LDHs@P-Nickel Foam Nano-array as High-Performance Supercapacitor Electrode. *J. Colloid. Interface Sci.* **2021**, *583*, 1–12.

42. Wu, D.J.; Han, H.C.; Hong, X.K.; Tao, S.; Xu, S.H.; Qian, B.; Wang, L.W.; Chen, X.F.; Chu, P.K. A Novel Self-branching $MnCo_2O_4$/nanographene Hybrid Composites on Macroporous Electrically Conductive Network as Bifunctional Electrodes for Boosting Miniature Supercapacitors and Sodium Ion Batteries. *J. Alloys Compd.* **2020**, *846*, 155720.
43. Saren, P.; Adhikari, A.D.; Khan, S.; Nayak, G.C. Self-Assembled GNS Wrapped Flower-like $MnCo_2O_4$ Nanostructures for Supercapacitor Application. *J. Solid State Chem.* **2019**, *271*, 282–291. [CrossRef]
44. Edison, T.N.J.I.; Atchudan, R.; Lee, Y.R. Facile Synthesis of Carbon Encapsulated RuO_2 Nanorods for Supercapacitor and Electrocatalytic Hydrogen Evolution Reaction. *Int. J. Hydrogen Energy* **2019**, *44*, 2323–2329. [CrossRef]
45. Ma, L.B.; Shen, X.P.; Zhou, H.; Ji, Z.Y.; Chen, K.M.; Zhu, G.X. High Performance Supercapacitor Electrode Materials Based on Porous $NiCo_2O_4$ Hexagonal Nanoplates/reduced Graphene Oxide Composites. *Chem. Eng. J.* **2015**, *262*, 980–988.
46. Lei, Y.; Li, J.; Wang, Y.Y.; Gu, L.; Chang, Y.F.; Yuan, H.Y.; Xiao, D. Rapid Microwave-assisted Green Synthesis of 3D Hierarchical Flower-shaped $NiCo_2O_4$ Microsphere for High-performance Supercapacitor. *ACS Appl. Mater. Inter.* **2014**, *6*, 1773–1780.
47. Liu, Y.J.; Zhang, X.; Matras-Postolek, K.; Yang, P. Ni_2P Nanosheets Modified N-doped Hollow Carbon Spheres towards Enhanced Supercapacitor Performance. *J. Alloys Compd.* **2020**, *854*, 157111.
48. Samuel, E.; Aldalbahi, A.; El-Newehy, M.; El-Hamshary, H.; Yoon, S.S. Nickel Ferrite Beehive-like Nanosheets for Binder-free and High-energy-storage Supercapacitor Electrodes. *J. Alloys Compd.* **2021**, *852*, 156929. [CrossRef]
49. Yi, M.J.; Lu, B.B.; Zhang, X.T.; Tan, Y.B.; Zhu, Z.Y.; Pan, Z.C.; Zhang, J.H. Ionic Liquid-assisted Synthesis of Nickel Cobalt Phosphide Embedded in N,P Codoped-carbon with Hollow and Folded Structures for Efficient Hydrogen Evolution Reaction and supercapacitor. *Appl. Catal. B.* **2021**, *283*, 119635.
50. Samuel, E.; Joshi, B.; Kim, Y.I.; Aldalbahi, A.; Rahaman, M.; Yoon, S.S. ZnO/MnO × Nanoflowers for High-Performance Supercapacitor Electrodes. *ACS Sustain. Chem. Eng.* **2020**, *8*, 3697–3708. [CrossRef]
51. Chen, H.Y.; Du, X.M.; Sun, J.L.; Wu, R.Z.; Wang, Y.; Xu, C.J. Template-free Synthesis of Novel Co_3O_4 Micro-bundles Assembled with Flakes for High-performance Hybrid Supercapacitors. *Ceram. Int.* **2021**, *47*, 716–724.
52. Dai, M.Z.; Zhao, D.P.; Wu, X. Research Progress on Transition Metal Oxide Based Electrode Materials for Asymmetric Hybrid Capacitors. *Chin. Chem. Lett.* **2020**, *31*, 2177–2188.
53. Hu, P.F.; Zhao, D.P.; Liu, H.Q.; Chen, K.F.; Xu, X. Engineering PPy decorated $MnCo_2O_4$ Urchins for Quasi-solid-state Hybrid Capacitors. *CrystEngComm* **2019**, *21*, 1600–1606.
54. Pawar, S.M.; Pawar, B.S.; Babar, P.T.; Ahmed, A.T.A.; Chavan, H.S.; Jo, Y.; Cho, S.; Kim, J.; Hou, B.; Inamdar, A.I.; et al. Nanoporous $CuCo_2O_4$ nanosheets as a Highly Efficient Bifunctional Electrode for Supercapacitors and Water Oxidation Catalysis. *Appl. Surf. Sci.* **2019**, *470*, 360–367. [CrossRef]
55. Babulal, S.M.; Venkatesh, K.; Chen, T.W.; Chen, S.W.; Krishnapandi, A.; Rwei, S.P.; Ramaraj, S.K. Synthesis of $MnMoO_4$ Nanorods by a Simple Co-Precipitation Method in Presence of Polyethylene Glycol for Pseudocapacitor Application. *Int. J. Electrochem. Sci.* **2020**, *15*, 7053–7063. [CrossRef]
56. Yu, F.; Pang, L.; Wang, H.-X. Preparation of Mulberry-like RuO_2 Electrode Material for Supercapacitors. *Rare Met.* **2021**, *40*, 440–447.
57. Xie, Y.B.; Yao, C. Electrochemical Performance of RuO_2-TiO_2 Nanotube Hybrid Electrode Material. *Mater. Res. Express* **2019**, *6*, 125550.
58. Xu, J.; Wang, Q.F.; Wang, X.W.; Xiang, Q.Y.; Liang, B.; Shen, G.Z. Flexible Asymmetric Supercapacitors Based upon Co_9S_8 Nanorod//CO_3O_4@RuO_2 Nanosheet Arrays on Carbon Cloth. *ACS Nano* **2013**, *7*, 5453–5462.
59. Manuraj, M.; Chacko, J.; Unni, K.N.N.; Rakhi, R.B. Heterostructured MoS_2-RuO_2 Nanocomposite: A Promising Electrode Material for Supercapacitors. *J. Alloys Compd.* **2020**, *836*, 155420. [CrossRef]
60. Park, S.; Shin, D.; Yeo, T.; Seo, B.; Hwang, H.; Lee, J.; Choi, W. Combustion-driven Synthesis Route for Tunable TiO_2/RuO_2 Hybrid Composites as High-performance Electrode Materials for Supercapacitors. *Chem. Eng. J.* **2020**, *384*, 123269.
61. Patil, A.M.; An, X.W.; Li, S.S.; Yue, X.Y.; Du, X.; Yoshida, A.; Hao, X.G.; Abudula, A.; Guan, G.Q. Fabrication of Three-dimensionally Heterostructured rGO/WO_3·0.5H_2O@Cu_2S Electrodes for High-energy Solid-state Pouch-type Asymmetric Supercapacitor. *Chem. Eng. J.* **2021**, *403*, 126411. [CrossRef]
62. Asim, S.; Javed, M.S.; Hussain, S.; Ran, M.; Iram, F.; Lv, D.D.; Hashim, M.; Jawaria, R.; Saleem, M.; Gul, N.; et al. RuO_2 Nanorods Decorated CNTs Grown Carbon Cloth as a Free Standing Electrode for Supercapacitor and Lithium Ion Batteries. *Electrochimica Acta* **2019**, *326*, 135009.
63. Zhu, D.H.; Zhou, Q.J.; Liang, A.Q.; Zhou, W.Q.; Chang, Y.N.; Li, D.Q.; Wu, J.; Ye, G.; Xu, J.K.; Ren, Y. Two-step Preparation of Carbon Nanotubes/RuO_2/polyindole Ternary Nanocomposites and Their Application as High-performance Supercapacitors. *Front. Mater. Sci.* **2020**, *14*, 109–119.
64. Zhang, P.; Liu, X.F.; He, H.W.; Peng, Y.J.; Wu, Y.H. Engineering RuO_2 on $CuCo_2O_4$/CuO Nanoneedles as Multifunctional Electrodes for the Hybrid Supercapacitors and Water Oxidation Catalysis. *J. Alloys Compd.* **2020**, *832*, 154962. [CrossRef]
65. Liu, S.Y.; Wang, R.C.; Ma, C.X.; Yang, D.H.; Li, D.X.; Lewandowski, Z. Improvement of Electrochemical Performance via Enhanced Reactive Oxygen Species Adsorption at ZnO–NiO@rGO Carbon Felt Cathodes in Photosynthetic Algal Microbial Fuel Cells. *Chem. Eng. J.* **2020**, *391*, 123627.
66. Wu, Z.S.; Wang, D.W.; Ren, W.; Zhao, J.; Zhou, G.; Li, F.; Cheng, H.M. Anchoring Hydrous RuO_2 on Graphene Sheets for High-performance Electrochemical Capacitors. *Adv. Funct. Mater.* **2010**, *20*, 3595–3602.

67. Jeon, S.; Jeong, J.H.; Yoo, H.; Yu, H.K.; Kim, B.H.; Kim, M.H. RuO_2 Nanorods on Electrospun Carbon Nanofibers for Supercapacitors. *ACS Appl. Nano Mater.* **2020**, *3*, 3847–3858.
68. Kim, Y.T.; Tadai, K.; Mitani, T. Highly Dispersed Ruthenium Oxide Nanoparticles on Carboxylated Carbon Nanotubes for Supercapacitor Electrode Materials. *J. Mater. Chem.* **2005**, *15*, 4914–4921.
69. Parker, S.F.; Robertson, S.J.; Imberti, S. Structure and Spectroscopy of the Supercapacitor Material Hydrous Ruthenium Oxide, RuO_2·xH2o, by Neutron Scattering. *Mol. Phys.* **2019**, *117*, 3417–3423. [CrossRef]
70. Hu, C.C.; Chen, W.C.; Chang, K.H. How to Achieve Maximum Utilization of Hydrous Ruthenium Oxide for Supercapacitors. *J. Electrochem. Soc.* **2004**, *151*, A281–A290.
71. Yang, L.; Zhang, J.M.; Zhang, Y.S.; Zhao, Y.L.; Yin, H.; Hua, Q.S.; Yuan, J.S.; Tang, J. A Ternary Composite RuO_2@SWCNT/graphene for High Performance Electrochemical Capacitors. *Mater. Lett.* **2020**, *259*, 126860.
72. Ji, S.-H.; Chodankar, N.R.; Kim, D.-H. Aqueous Asymmetric Supercapacitor Based on RuO_2-WO_3 Electrodes. *Electrochim. Acta* **2019**, *325*, 134879.
73. Jiang, Q.; Kurra, N.; Alhabeb, M.; Gogotsi, Y.; Alshareef, H.N. All Pseudocapacitive MXene-RuO_2 Asymmetric Supercapacitors. *Adv. Energy Mater.* **2018**, *8*, 1703043. [CrossRef]
74. Zhang, C.; Xiao, J.; Qian, L.H.; Lv, X.L.; Yuan, S.L.; Wang, S.; Lei, P.X. Hierarchically Porous Co_3O_4/C Nanowire Arrays Derived from a Metal–organic Framework for High Performance Supercapacitors and the Oxygen Evolution Reaction. *J. Mater. Chem. A* **2016**, *4*, 16516–16523. [CrossRef]
75. Adhikari, S.; Selvaraj, S.; Ji, S.H.; Kim, D.H. Encapsulation of Co_3O_4 Nanocone Arrays via Ultrathin NiO for Superior Performance Asymmetric Supercapacitors. *Small* **2020**, *16*, 2005414. [CrossRef]
76. Wang, X.L.; Fu, J.W.; Wang, Q.F.; Dong, Z.J.; Wang, X.L.; Hu, A.Y.; Wang, W.; Yang, S.B. Preparation and Electrochemical Properties of Co_3O_4 Supercapacitor Electrode Materials. *Crystals* **2020**, *10*, 720.
77. Liao, Q.Y.; Li, N.; Jin, S.X.; Yang, G.W.; Wang, C.X. All-solid-state Symmetric Supercapacitor Based on Co_3O_4 Nanoparticles on Vertically Aligned Graphene. *ACS Nano* **2015**, *9*, 5310–5317.
78. Wang, X.M.; Yin, S.M.; Jiang, J.; Xiao, H.P.; Li, X.H. A Tightly Packed Co_3O_4/C&S Composite for High-performance Electrochemical Supercapacitors from a Cobalt (III) Cluster-based Coordination Precursor. *J. Solid State Chem.* **2020**, *288*, 121435.
79. Lu, J.L.; Li, J.E.; Wan, J.; Han, X.Y.; Ji, P.Y.; Luo, S.; Gu, M.X.; Wei, D.P.; Hu, C.G. A Facile Strategy of In-situ Anchoring of Co_3O_4 on N Doped Carbon Cloth for an Ultrahigh Electrochemical Performance. *Nano Res.* **2020**, 1–8. [CrossRef]
80. Chatterjee, M.; Sain, S.; Roy, A.; Das, S.; Pradhan, S.W. Enhanced Electrochemical Properties of Co_3O_4 with Morphological Hierarchy for Energy Storage Application: A Comparative Study with Different Electrolytes. *J. Phys. Chem. Solids* **2021**, *148*, 109733. [CrossRef]
81. Cao, J.M.; Li, J.Z.; Zhou, L.; Xi, Y.L.; Cao, X.; Zhang, Y.M.; Han, W. Tunable Agglomeration of Co_3O_4 Nanowires as the Growing Core for In-situ Formation of Co_2NiO_4 Assembled with Polyaniline-derived Carbonaceous Fibers as the High-performance Asymmetric Supercapacitors. *J. Alloys Compd.* **2021**, *853*, 157210.
82. Deng, J.C.; Kang, L.T.; Bai, G.L.; Li, Y.; Li, P.Y.; Liu, X.G.; Yang, Y.Z.; Gao, F.; Liang, W. Solution Combustion Synthesis of Cobalt Oxides (Co_3O_4 and Co_3O_4/CoO) Nanoparticles as Supercapacitor Electrode Materials. *Electrochim. Acta* **2014**, *132*, 127–135.
83. Xiang, C.C.; Li, M.; Zhi, M.J.; Manivannan, A.; Wu, N.Q. A reduced Graphene Oxide/Co_3O_4 Composite for Supercapacitor Electrode. *J. Power Sources* **2013**, *226*, 65–70. [CrossRef]
84. Kumar, R.; Youssry, S.M.; Soe, H.M.; Abdel-Galeil, M.M.; Kawamura, G.; Matsuda, A. Honeycomb-like Open-edged Reduced-graphene-oxide-enclosed Transition Metal Oxides (NiO/Co_3O_4) as Improved Electrode Materials for High-performance Supercapacitor. *J. Energy Storage* **2020**, *30*, 101539. [CrossRef]
85. Ji, Z.Y.; Liu, K.; Li, N.; Zhang, H.Y.; Dai, W.Y.; Shen, X.P.; Zhu, G.X.; Kong, L.R.; Yuan, A.H. Nitrogen-doped Carbon Dots Anchored NiO/Co_3O_4 Ultrathin Nanosheets as Advanced Cathodes for Hybrid Supercapacitors. *J. Colloid Interface Sci.* **2020**, *579*, 282–289.
86. Yue, X.-M.; Liu, Z.-J.; Xiao, C.-C.; Ye, M.; Peng, C.; Gu, Z.-Y.; Zhu, J.-S.; Zhang, S.-Q. Synthesis of Co_3O_4/reduced Graphene Oxide by One Step-hydrothermal and Calcination Method for High-performance Supercapacitors. *Ionics* **2021**, *27*, 339–349.
87. Zhao, Y.; Liu, H.Q.; Hu, P.F.; Song, J.R.; Xiao, L. Asymmetric Hybrid Capacitor Based on Co_3O_4 Nanowire Electrode. *Ionics* **2020**, *26*, 6289–6295.
88. Priyadharsini, C.I.; Marimuthu, G.; Pazhanivel, T.; Anbarasan, P.M.; Aroulmoji, V.; Mohana, L. Sol–Gel Synthesis of Co_3O_4 Nanoparticles as an Electrode Material for Supercapacitor Applications. *J. Sol. Gel Sci. Technol.* **2020**, *96*, 416–422. [CrossRef]
89. Guan, C.; Liu, X.M.; Ren, W.N.; Li, X.; Cheng, C.W.; Wang, J. Rational Design of Metal-organic Framework Derived Hollow $NiCo_2O_4$ Arrays for Flexible Supercapacitor and Electrocatalysis. *Adv. Energy Mater.* **2017**, *7*, 1602391.
90. Aadil, M.; Zulfiqar, S.; Shahid, M.; Haider, S.; Shakir, I.; Warsi, M.F. Binder Free Mesoporous Ag-doped Co_3O_4 Nanosheets with Outstanding Cyclic Stability and Rate Capability for Advanced Supercapacitor Applications. *J. Alloys Compd.* **2020**, *844*, 156062. [CrossRef]
91. Yang, X.Y.; Xiang, C.L.; Zou, Y.J.; Liang, J.; Zhang, H.Z.; Yan, E.H.; Xu, F.; Hu, X.B.; Cheng, Q.; Sun, L.X. Low-temperature Synthesis of Sea Urchin-like Co-Ni Oxide on Graphene Oxide for Supercapacitor Electrodes. *J. Mater. Sci. Technol.* **2020**, *55*, 223–230.
92. Wang, Z.W.; Zhao, K.M.; Lu, S.X.; Xu, W.G. Application of Flammulina-velutipes-like CeO_2/Co_3O_4/rGO in High-performance Asymmetric Supercapacitors. *Electrochim. Acta* **2020**, *353*, 136599.

93. Wei, G.; Yan, L.Q.; Huang, H.F.; Yan, F.X.; Liang, X.Q.; Xu, S.K.; Lan, Z.Q.; Zhou, W.Z.; Guo, J. The Hetero-structured Nanoarray Construction of Co_3O_4 Nanowires Anchored on Nanoflakes as a High-performance Electrode for Supercapacitors. *Appl. Surf. Sci.* **2021**, *538*, 147932.
94. Cheng, L.; Zhang, Q.S.; Xu, M.; Zhai, Q.C.; Zhang, C.L. Two-for-one Strategy: Three-dimensional Porous Fe-doped Co_3O_4 Cathode and N-doped Carbon Anode Derived from a Single Bimetallic Metal-organic Framework for Enhanced Hybrid Supercapacitor. *J. Colloid Interface Sci.* **2021**, *583*, 299–309. [CrossRef] [PubMed]
95. Gong, Y.J.; An, J.N.; Dai, H.B.; Chen, R.Y.; Yu, C.Y.; Chen, Q.; Zhou, J.Y.; Sun, G.Z.; Huang, W. Hierarchically Tubular Architectures Composed of Vertical Carbon Nanosheets Embedded with Oxygen-vacancy Enriched Hollow Co_3O_4 Nanoparticles for Improved Energy Storage. *Electrochim. Acta* **2020**, *356*, 136843.
96. Saraf, M.; Rajak, R.; Mobin, S.M. MOF Derived High Surface Area Enabled Porous Co_3O_4 Nanoparticles for Supercapacitors. *ChemistrySelect* **2019**, *4*, 8142–8149. [CrossRef]
97. Bao, Y.X.; Deng, Y.; Wang, M.Z.; Xiao, Z.Y.; Wang, M.H.; Fu, Y.L.; Guo, Z.Y.; Yang, Y.; Wang, L. A Controllable Top-down Etching and In-situ Xxidizing Strategy: Metal-organic Frameworks Derived α-Co/$Ni(OH)_2$@Co_3O_4 Hollow Nanocages for Enhanced Supercapacitor Performance. *Appl. Surf. Sci.* **2020**, *504*, 144395.
98. Wei, G.J.; Zhou, Z.; Zhao, X.X.; Zhang, W.Q.; An, C.H. Ultrathin Metal–organic Framework Nanosheet-derived Ultrathin Co_3O_4 Nanomeshes with Robust Oxygen-evolving Performance and Asymmetric Supercapacitors. *ACS Appl. Mater. Interf.* **2018**, *10*, 23721–23730.
99. Dai, S.M.; Han, F.F.; Tang, J.; Tang, W.H. MOF-derived Co_3O_4 Nanosheets Rich in Oxygen Vacancies for Efficient All-solid-state Symmetric Supercapacitors. *Electrochim. Acta* **2019**, *328*, 135103.
100. Li, S.M.; Yang, K.; Ya, P.; Ma, K.R.; Zhang, Z.; Huang, Q. Three-dimensional Porous Carbon/Co_3O_4 Composites Derived from Graphene/Co-MOF for High Performance Supercapacitor Electrodes. *Appl. Surf. Sci.* **2020**, *503*, 144090.
101. Zhang, L.J.; Zhang, Y.Y.; Huang, S.L.; Yuan, Y.L.; Li, H.; Jin, Z.Y.; Wu, J.H.; Liao, Q.F.; Hu, L.; Lu, J.G.; et al. Co_3O_4/Ni-based MOFs on Carbon Cloth for Flexible Alkaline Battery-supercapacitor Hybrid Devices and Near-infrared Photocatalytic Hydrogen Evolution. *Electrochim. Acta* **2018**, *281*, 189–197. [CrossRef]
102. Han, D.D.; Wei, J.H.; Zhao, Y.; Shen, Y.; Pan, Y.F.; Wei, F.; Mao, L.C. Metal–organic Framework Derived Petal-like Co_3O_4@$CoNi_2S_4$ Hybrid on Carbon Cloth with Enhanced Performance for Supercapacitors. *Inorg. Chem. Front.* **2020**, *7*, 1428–1436.
103. Huang, Y.Y.; Bao, S.; Lu, J.L. Flower-like MnO_2/polyaniline/hollow Mesoporous Silica as Electrode for High-performance All-solid-state Supercapacitors. *J. Alloys Compd.* **2020**, *845*, 156192. [CrossRef]
104. Noh, J.; Yoon, C.M.; Kim, Y.K.; Jang, J. High Performance Asymmetric Supercapacitor Twisted from Carbon Fiber/MnO_2 and Carbon Fiber/MoO_3. *Carbon* **2017**, *116*, 470–478.
105. Raut, S.D.; Mane, H.R.; Shinde, N.M.; Lee, D.; Shaikh, S.F.; Kim, K.H.; Kim, H.-J.; Al-Enizi, A.M.; Mane, R.S. Electrochemically Grown MnO_2 Nanowires for Supercapacitor and Electrocatalysis Applications. *New J. Chem.* **2020**, *44*, 17864–17870.
106. Lu, W.; Li, Y.; Yang, M.; Jiang, X.; Zhang, Y.X.; Xing, Y. Construction of Hierarchical Mn_2O_3@MnO_2 Core–Shell Nanofibers for Enhanced Performance Supercapacitor Electrodes. *ACS Appl. Energy Mater.* **2020**, *3*, 8190–8197.
107. Rani, J.R.; Thangavel, R.; Kim, M.; Lee, Y.S.; Jang, J.H. Ultra-High Energy Density Hybrid Supercapacitors Using MnO_2/Reduced Graphene Oxide Hybrid Nanoscrolls. *Nanomaterials* **2020**, *10*, 2049.
108. Liu, P.B.; Zhu, Y.D.; Gao, X.G.; Huang, Y.; Wang, Y.; Qin, S.Y.; Zhang, Y.Q. Rational Construction of Bowl-like MnO_2 Nanosheets with Excellent Electrochemical Performance for Supercapacitor Electrodes. *Chem. Eng. J.* **2018**, *350*, 79–88.
109. Wang, Q.F.; Ma, Y.; Liang, X.; Zhang, D.H.; Miao, M.H. Flexible Supercapacitors Based on Carbon Nanotube-MnO_2 Nanocomposite Film Electrode. *Chem. Eng. J.* **2019**, *371*, 145–153.
110. Wu, K.Q.; Ye, Z.G.; Ding, Y.; Zhu, Z.X.; Peng, X.Y.; Li, D.S.; Ma, G. Facile Co-deposition of the Carbon@MnO_2 Heterostructure for High-performance Flexible Supercapacitors. *J. Power Sources* **2020**, *477*, 229031.
111. Zhao, Y.F.; Ran, W.; He, J.; Huang, Y.Z.; Liu, Z.F.; Liu, W.; Tang, Y.F.; Zhang, L.; Gao, D.W.; Gao, F.M. High-performance Asymmetric Supercapacitors Based on Multilayer MnO_2/graphene Oxide Nanoflakes and Hierarchical Porous Carbon with Enhanced Cycling Stability. *Small* **2015**, *11*, 1310–1319.
112. Wang, L.; Ouyang, Y.; Jiao, X.Y.; Xia, X.F.; Lei, W.; Hao, Q.L. Polyaniline-assisted Growth of MnO_2 Ultrathin Nanosheets on Graphene and Porous Graphene for Asymmetric Supercapacitor with Enhanced Energy Density. *Chem. Eng. J.* **2018**, *334*, 1–9.
113. Bose, N.; Sundararajan, V.; Prasankumar, T.; Jose, S.P. α–MnO_2 Coated Anion Intercalated Carbon Nanowires: A High Rate Capability Electrode Material for Supercapacitors. *Mater. Lett.* **2020**, *278*, 128457.
114. Sui, Z.Y.; Chang, Z.S.; Xu, X.F.; Li, Y.L.; Zhu, X.M.; Zhao, C.; Chen, Q. Direct Growth of MnO_2 on Highly Porous Nitrogen-doped Carbon Nanowires for Asymmetric Supercapacitors. *Diam. Relat. Mater.* **2020**, *108*, 107988.
115. Cakici, M.; Reddy, K.R.; Alonso-Marroquin, F. Advanced Electrochemical Energy Storage Supercapacitors Based on the Flexible Carbon Fiber Fabric-coated with Uniform Coral-like MnO_2 Structured Electrodes. *Chem. Eng. J.* **2017**, *309*, 151–158. [CrossRef]
116. Zhao, P.; Yao, M.Q.; Ren, H.B.; Wang, N.; Komarneni, S. Nanocomposites of Hierarchical Ultrathin MnO_2 Nanosheets/hollow Carbon Nanofibers for High-performance Asymmetric Supercapacitors. *Appl. Surf. Sci.* **2019**, *463*, 931–938.
117. Cai, W.R.; Kankala, R.K.; Xiao, M.T.; Zhang, N.; Zhang, X.Q. Three-dimensional Hollow N-doped ZIF-8-derived Carbon@MnO_2 Composites for Supercapacitors. *Appl. Surf. Sci.* **2020**, *528*, 146921.

118. Long, X.; Tian, L.; Zhang, L.; Wang, J.; Chen, Y.; Emin, A.; Wang, X.; Xie, W.L.; Liu, D.Q.; Fu, Y.J.; et al. Interconnected δ-MnO_2 Nanosheets Anchored on Activated Carbon Cloth as Flexible Electrode for High-performance Aqueous Asymmetric Supercapacitors. *J. Electroanal. Chem.* **2020**, *877*, 114656.
119. Lei, R.; Gao, J.H.; Qi, L.F.; Ye, L.L.; Wang, C.; Le, Y.; Huang, Y.; Shi, X.G.; Ni, H.W. Construction of MnO_2 Nanosheets@graphenated Carbon Nanotube Networks Core-shell Heterostructure on 316L Stainless Steel as Binder-free Supercapacitor Electrodes. *Int. J. Hydrogen Energy* **2020**, *45*, 28930–28939.
120. Bai, X.L.; Gao, Y.L.; Gao, Z.Y.; Ma, J.Y.; Tong, X.L.; Sun, H.B.; Wang, J.A. Supercapacitor Performance of 3D-graphene/MnO_2 Foam Synthesized via the Combination of Chemical Vapor Deposition with Hydrothermal Method. *Appl. Phys. Lett.* **2020**, *117*, 183901.
121. Xiong, C.Y.; Yang, Q.; Dang, W.H.; Li, M.R.; Li, B.B.; Su, J.; Liu, Y.; Zhao, W.; Duan, C.; Dai, L.; et al. Fabrication of Eco-friendly Carbon Microtubes@nitrogen-doped Reduced Graphene Oxide Hybrid as an Excellent Carbonaceous Scaffold to Load MnO_2 Nanowall (PANI nanorod) as Bifunctional Material for High-performance Supercapacitor and Oxygen Reduction Reaction Catalyst. *J. Power Sources* **2020**, *447*, 227387.
122. Li, M.L.; Yu, J.; Wang, X.D.; Yang, Z.L. 3D Porous MnO_2@carbon Nanosheet Synthesized from Rambutan Peel for High-performing Supercapacitor Electrodes Materials. *Appl. Surf. Sci.* **2020**, *530*, 147230.
123. Huang, R.; Zhou, R.H.; Wang, L.; Zhu, Y.M. Dandelion-like CoO/Co_3O_4/Carbon Composites as Anode Materials for a High-Performance Lithium Ion Battery. *ChemistrySelect* **2020**, *5*, 12932–12939. [CrossRef]
124. Shen, H.J.; Kong, X.D.; Zhang, P.; Song, X.L.; Wang, H.; Zhang, Y. In-situ Hydrothermal Synthesis of δ-MnO_2/soybean Pod Carbon and Its High Performance Application on Supercapacitor. *J. Alloys Compd.* **2021**, *853*, 157357.
125. Du, W.; Wang, X.N.; Zhan, J.; Sun, X.Q.; Kang, L.T.; Jiang, F.Y.; Zhang, X.Y.; Shao, Q.; Dong, M.Y.; Liu, H.; et al. Biological Cell Template Synthesis of Nitrogen-doped Porous Hollow Carbon Spheres/MnO_2 Composites for High-performance Asymmetric Supercapacitors. *Electrochim. Acta* **2019**, *296*, 907–915.
126. Nie, G.D.; Luan, Y.X.; Kou, Z.K.; Jiang, J.M.; Zhang, Z.Y.; Yang, N.; Wang, J.; Long, Y.-Z. Fiber-in-tube and Particle-in-tube Hierarchical Nanostructures Enable High Energy Density of MnO_2-based Asymmetric Supercapacitors. *J. Colloid Interface Sci.* **2021**, *582*, 543–551.
127. Yi, T.F.; Mei, J.; Guan, B.L.; Cui, P.; Luo, S.H.; Xie, Y.; Liu, Y.G. Construction of Spherical NiO@MnO_2 with Core-shell Structure Obtained by Depositing MnO_2 Nanoparticles on NiO Nanosheets for High-performance Supercapacitor. *Ceram. Int.* **2020**, *46*, 421–429.
128. Liu, G.; Ma, L.; Liu, Q.M. The Preparation of Co_3O_4@MnO_2 Hierarchical Nano-sheets for High-output Potential Supercapacitors. *Electrochim. Acta* **2020**, *364*, 137265.
129. Zhao, Y.; He, J.F.; Dai, M.Z.; Zhao, D.P.; Wu, X.; Liu, B.D. Emerging CoMn-LDH@MnO_2 Electrode Materials Assembled Using Nanosheets for Flexible and Foldable Energy Storage Devices. *J. Energy Chem.* **2020**, *45*, 67–73.
130. Chen, X.Y.; Wang, X.Z.; Liu, F.J.; Song, X.J.; Cui, H.Z. Fabrication of NiO–ZnO-modified g-C3N4 Hierarchical Composites for High-performance Supercapacitors. *Vacuum* **2020**, *178*, 109453.
131. Murali, S.; Dammala, P.K.; Rani, B.; Santhosh, R.; Jadhao, C.; Sahu, N.K. Polyol Mediated Synthesis of Anisotropic ZnO Nanomaterials and Composite with rGO: Application towards Hybrid Supercapacitor. *J. Alloys Compd.* **2020**, *844*, 156149. [CrossRef]
132. Ouyang, Y.; Xia, X.F.; Ye, H.T.; Wang, L.; Jiao, X.Y.; Lei, W.; Hao, Q.L. Three-dimensional Hierarchical Structure ZnO@C@NiO on Carbon Cloth for Asymmetric Supercapacitor with Enhanced Cycle Stability. *ACS Appl. Mater. Interfaces* **2018**, *10*, 3549–3561. [CrossRef]
133. Angelin, M.D.; Rajkumar, S.; Merlin, J.P.; Xavier, A.R.; Franklin, M.; Ravichandran, A.T. Electrochemical Investigation of Zr-doped ZnO Nanostructured Electrode Material for High-performance Supercapacitor. *Ionics* **2020**, *26*, 5757–5772. [CrossRef]
134. Naeem, F.; Naeem, S.; Zhao, Z.; Shu, G.Q.; Zhang, J.; Mei, Y.F.; Huang, G.S. Atomic Layer Deposition Synthesized ZnO Nanomembranes: A Facile Route towards Stable Supercapacitor Electrode for High Capacitance. *J. Power Sources* **2020**, *451*, 227740. [CrossRef]
135. Miah, M.; Mondal, T.K.; Ghosh, A.; Saha, S.K. Study of Highly Porous ZnO Nanospheres Embedded Reduced Graphene Oxide for High Performance Supercapacitor Application. *Electrochim. Acta* **2020**, *354*, 136675.
136. Liu, J.; Xu, T.; Sun, X.W.; Bai, J.; Li, C.P. Preparation of Stable Composite Porous Nanofibers Carried SnO_x-ZnO as a Flexible Supercapacitor Material with Excellent Electrochemical and Cycling Performance. *J. Alloys Compd.* **2019**, *807*, 151652.
137. Kumar, R.; Youssry, S.M.; Abdel-Galeil, M.M.; Matsuda, A. One-pot Synthesis of Reduced Graphene Oxide Nanosheets Anchored ZnO Nanoparticles via Microwave Approach for Electrochemical Performance as Supercapacitor Electrode. *J. Mater. Sci.-Mater. Electron.* **2020**, *31*, 15456–15465. [CrossRef]
138. Chaudhary, S.; James, L.S.; Kumar, A.B.V.K.; Ramana, C.V.V.; Mishra, D.K.; Thomas, S.; Kim, D. Reduced Graphene Oxide/ZnO Nanorods Nanocomposite: Structural, Electrical and Electrochemical Properties. *J. Inorg. Organomet. Polym. Mater.* **2019**, *29*, 2282–2290. [CrossRef]
139. Wang, W.; Jiao, S.S.; Cao, J.Y.; Naguib, H.E. Zinc Oxide/carbon Nanotube Nanocomposite for High-performance Flexible Supercapacitor with Sensing Ability. *Electrochim. Acta* **2020**, *350*, 136353.
140. Arunpandiyan, S.; Bharathi, S.; Pandikumar, A.; Arasi, S.E.; Arivarasan, A. Structural Analysis and Redox Additive Electrolyte Based Supercapacitor Performance of ZnO/CeO_2 Nanocomposite. *Mat. Sci. Semicon. Proc.* **2020**, *106*, 104765. [CrossRef]

141. Shaheen, I.; Ahmad, K.S.; Zequine, C.; Gupta, R.K.; Thomas, A.G.; Malik, M.A. Green Synthesis of ZnO-Co_3O_4 Nanocomposite Using Facile Foliar Fuel and Investigation of Its Electrochemical Behaviour for Supercapacitors. *New J. Chem.* **2020**, *44*, 18281–18292. [CrossRef]
142. Zhou, H.Y.; Fu, W.B.; Muhammad, M.; Xie, M.Z.; Xie, E.Q.; Han, W.H. Self-assembled Microspheres Composed of Porous ZnO/CoO Nanosheets for Aqueous Hybrid Supercapacitors. *J. Phys. D Appl. Phys.* **2019**, *52*, 505501.
143. Chakraborty, S.; Raj, M.A.; Mary, N.L. Biocompatible Supercapacitor Electrodes Using Green Synthesised ZnO/Polymer Nanocomposites for Efficient Energy Storage Applications. *J. Energy Storage* **2020**, *28*, 101275. [CrossRef]
144. Simon, R.; Chakraborty, S.; Konikkara, N.; Mary, N.L. Functionalized Polystyrene Maleic Anhydride Copolymer/ZnO Nanocomposites for Enhanced Electrochemical Performance. *J. Appl. Polym. Sci.* **2020**, *137*, 48945. [CrossRef]
145. He, X.J.; Li, X.J.; Ma, H.; Han, J.F.; Zhang, H.; Yu, C.; Xiao, N.; Qiu, J.S. ZnO Template Strategy for the Synthesis of 3D Interconnected Graphene Nanocapsules from Coal Tar Pitch as Supercapacitor Electrode Materials. *J. Power Sources* **2017**, *340*, 183–191.
146. Chebrolu, V.T.; Balakrishnan, B.; Cho, I.; Bak, J.S.; Kim, H.J. A Unique Core-shell Structured ZnO/NiO Heterojunction to Improve the Performance of Supercapacitors Produced Using a Chemical Bath Deposition Approach. *Dalton Trans.* **2020**, *49*, 14432–14444. [CrossRef]
147. Di, S.; Gong, L.G.; Zhou, B.B. Precipitated Synthesis of Al_2O_3-ZnO Nanorod for High-Performance Symmetrical Supercapacitors. *Mater. Chemi. Phys.* **2020**, *253*, 123289.
148. Liu, X.J.; Liu, H.; Sun, X.Z. Aligned ZnO nanorod@Ni–Co Layered Double Hydroxide Composite Nanosheet Arrays with a Core–shell Structure as High-performance Supercapacitor Electrode Materials. *CrystEngComm* **2020**, *22*, 1593–1601.
149. Obodo, R.M.; Nwanya, A.C.; Arshad, M.; Iroegbu, C.; Ahmad, I.; Osuji, R.U.; Maaza, M.; Ezema, F.I. Conjugated NiO-ZnO/GO Nanocomposite Powder for Applications in Supercapacitor Electrodes Material. *Int. J. Energy Res.* **2020**, *44*, 3192–3202. [CrossRef]
150. Asgar, H.; Deen, K.M.; Haider, W. Estimation of Electrochemical Charge Storage Capability of ZnO/CuO/reduced Graphene Oxide Nanocomposites. *Int. J. Energy Res.* **2020**, *44*, 1580–1593. [CrossRef]
151. Obodo, R.M.; Asjad, M.; Nwanya, A.C.; Ahmad, I.; Zhao, T.K.; Ekwealor, A.B.C.; Ejikeme, P.M.; Maaza, M.; Ezema, F.I. Evaluation of 8.0 MeV Carbon (C^{2+}) Irradiation Effects on Hydrothermally Synthesized Co_3O_4-CuO-ZnO@GO Electrodes for Supercapacitor Applications. *Electroanaly* **2020**, *32*, 2958–2968. [CrossRef]
152. Yao, D.; Wang, F.L.; Lei, W.; Hua, Y.; Xia, X.F.; Liu, J.P.; Hao, Q.L. Oxygen Vacancies Boosting Ultra-stability of Mesoporous ZnO-CoO@N-doped Carbon Microspheres for Asymmetric Supercapacitors. *Sci. China Mater.* **2020**, *63*, 2013–2027.
153. Chen, H.C.; Lyu, Y.R.; Fang, A.; Lee, G.J.; Karuppasamy, L.; Wu, J.J.; Lin, C.K.; Ananda, S.; Chen, C.Y. The Design of ZnO Nanorod Arrays Coated with MnO_x for High Electrochemical Stability of a Pseudocapacitor Electrode. *Nanomaterials* **2020**, *10*, 475.
154. Sun, L.; Zhang, Y.X.; Si, H.C.; Shi, Y.; Sun, C.; Zhang, Y.H. Porous Mo-C Coverage on ZnO Rods for Enhanced Supercapacitive Performance. *Dalton Trans.* **2020**, *49*, 5134–5142.
155. Mohamed, I.M.A.; Yasin, A.S.; Liu, C.K. Synthesis, Surface Characterization and Electrochemical Performance of Zno@activated Carbon as a Supercapacitor Electrode Material in Acidic and Alkaline Electrolytes. *Ceram. Int.* **2020**, *46*, 3912–3920. [CrossRef]
156. He, D.; Wan, J.N.; Liu, G.L.; Suo, H.; Zhao, C. Design and Construction of Hierarchical α-$Co(OH)_2$-coated Ultra-thin ZnO Flower Nanostructures on Nickel Foam for High Performance Supercapacitors. *J. Alloys Compd.* **2020**, *838*, 155556.
157. Ding, S.X.; Li, X.Y.; Jiang, X.L.; Hu, Q.; Yan, Y.Q.; Zheng, Q.J. Core-shell Nanostructured ZnO@CoS Arrays as Advanced Electrode Materials for High-performance Supercapacitors. *Electrochim. Acta* **2020**, *354*, 136711.
158. Li, Z.L.; Sui, Y.W.; Qi, J.Q.; Wei, F.X.; He, Y.Z.; Meng, Q.K.; Ren, Y.J.; Zhang, X.P.; Zhan, Z.Z.; Sun, Z. 3D Core-shell Pistil-like $MnCo_2O_{4.5}$/polyaniline Nanocomposites as High Performance Supercapacitor Electrodes. *Compos. Interface* **2020**, *27*, 631–644.
159. Wang, H.Z.; Shen, C.; Liu, J.; Zhang, W.G.; Yao, S.W. Three-dimensional $MnCo_2O_4$/graphene Composites for Supercapacitor with Promising Electrochemical Properties. *J. Alloys Compd.* **2019**, *792*, 122–129.
160. Shanmugavadivel, M.; Dhayabaran, V.V.; Subramanian, M. Fabrication of High Energy and High Power Density Supercapacitor Based on $MnCo_2O_4$ Nanomaterial. *J. Phys. Chem. Solids* **2019**, *133*, 15–20. [CrossRef]
161. Maile, N.C.; Shinde, S.K.; Patil, R.T.; Fulari, A.V.; Kolim, R.R.; Kim, D.-Y.; Lee, D.S.; Fulari, V.J. Structural and Morphological Changes in Binder-free $MnCo_2O_4$ Electrodes for Supercapacitor Applications: Effect of Deposition Parameters. *J. Mater. Sci. Mater. Electron.* **2019**, *30*, 3729–3743. [CrossRef]
162. Wang, N.; Sun, B.L.; Zhao, P.; Yao, M.Q.; Hu, W.C.; Komarneni, S. Electrodeposition Preparation of $NiCo_2O_4$ Mesoporous Film on Ultrafine Nickel Wire for Flexible Asymmetric Supercapacitors. *Chem. Eng. J.* **2018**, *345*, 31–38.
163. Wang, X.; Xu, L.; Song, K.; Yane, R.; Jia, L.H.; Guo, X.F.; Jing, X.Y.; Wang, J. Synthesis of $MnCo_2O_4$@$MnCo_2S_4$ Core/shell Micro-nanostructures on Ni Foam for High Performance Asymmetric Supercapacitors. *Colloid Surf. A* **2019**, *570*, 73–80.
164. Xu, K.B.; Li, W.Y.; Liu, Q.; Li, B.; Liu, X.J.; An, L.; Chen, Z.G.; Zou, R.J.; Hu, J.Q. Hierarchical Mesoporous $NiCo_2O_4$@MnO_2 Core–shell Nanowire Arrays on Nickel Foam for Aqueous Asymmetric Supercapacitors. *J. Mater. Chem. A* **2014**, *2*, 4795–4802.
165. Zhu, D.; Sun, X.; Yu, J.; Liu, Q.; Liu, J.Y.; Chen, R.R.; Zhang, H.S.; Li, R.M.; Yu, J.; Wang, J. Rationally Designed $CuCo_2O_4$@$Ni(OH)_2$ with 3D Hierarchical Core-shell Structure for Flexible Energy Storage. *J. Colloid Interface Sci.* **2019**, *557*, 76–83.
166. Zhao, D.P.; Dai, M.Z.; Liu, H.Q.; Xiao, L.; Wu, X.; Xia, H. Constructing High Performance Hybrid Battery and Electrocatalyst by Heterostructured $NiCo_2O_4$@NiWS Nanosheets. *Cryst. Growth Des.* **2019**, *19*, 1921–1929.
167. Liu, Q.; Hong, X.D.; Zhang, X.; Wang, W.; Guo, W.X.; Liu, X.Y.; Ye, M.D. Hierarchically Structured Co_9S_8@$NiCo_2O_4$ Nanobrushes for High-performance Flexible Asymmetric Supercapacitors. *Chem. Eng. J.* **2019**, *356*, 985–993.

168. Xu, X.W.; Liu, Y.; Dong, P.; Ajayan, P.M.; Shen, J.F.; Ye, M.X. Mesostructured $CuCo_2S_4/CuCo_2O_4$ Nanoflowers as Advanced Electrodes for Asymmetric Supercapacitors. *J. Power Sources* **2018**, *400*, 96–103.
169. Liu, H.Y.; Guo, Z.X.; Wang, S.B.; Xun, X.C.; Chen, D.; Lian, J.S. Reduced Core-shell Structured $MnCo_2O_4$@MnO_2 Nanosheet Arrays with Oxygen Vacancies Grown on Ni Foam for Enhanced-performance Supercapacitors. *J. Alloys Compd.* **2020**, *846*, 156504.
170. Feng, Y.M.; Liu, W.F.; Wang, Y.; Gao, W.N.; Li, J.T.; Liu, K.L.; Wang, X.P.; Jiang, J. Oxygen Vacancies Enhance Supercapacitive Performance of $CuCo_2O_4$ in High-energy-density Asymmetric Supercapacitors. *J. Power Sources* **2020**, *458*, 228005.
171. Yan, D.; Wang, W.; Luo, X.; Chen, C.; Zeng, Y.; Zhu, Z.H. $NiCo_2O_4$ with Oxygen Vacancies as Better Performance Electrode Material for Supercapacitor. *Chem. Eng. J.* **2018**, *334*, 864–872.
172. Chen, T.; Shi, R.; Zhang, Y.Y.; Wang, Z.H. A $MnCo_2O_4$@$NiMoO_4$ Core-Shell Composite Supported on Nickel Foam as a Supercapacitor Electrode for Energy Storage. *ChemPlusChem* **2019**, *84*, 69–77.
173. Gao, Y.F.; Xia, Y.C.; Wan, H.J.; Xu, X.; Jiang, S. Enhanced Cycle Performance of Hierarchical Porous Sphere $MnCo_2O_4$ for Asymmetric Supercapacitors. *Electrochim. Acta* **2019**, *301*, 294–303.
174. Zhao, Y.H.; Dong, H.X.; He, X.Y.; Yu, J.; Chen, R.R.; Liu, Q.; Liu, J.Y.; Zhang, H.S.; Yu, J.; Wang, J. Carbon Cloth Modified with Metal-Organic Framework Derived CC@$CoMoO_4$-$Co(OH)_2$ Nanosheets Array as a Flexible Energy-Storage Material. *ChemElectroChem* **2019**, *6*, 3355–3366.
175. Daneshvar, S.; Arvand, M. In-situ Growth of Hierarchical Ni-Co LDH/$CoMoO_4$ Nanosheets Arrays on Ni Foam for Pseudocapacitors with Robust Cycle Stability. *J. Alloys Compd.* **2020**, *815*, 152421. [CrossRef]
176. Liu, H.Q.; Zhao, D.P.; Liu, Y.; Hu, P.F.; Wu, X.; Xia, H. Boosting Energy Storage and Electrocatalytic Performances by Synergizing $CoMoO_4$@$MoZn_{22}$ Core-shell Structures. *Chem. Eng. J.* **2019**, *373*, 485–492.
177. Chen, H.; Hu, H.M.; Han, F.; Liu, J.D.; Zhang, Y.R.; Zheng, Y.H. $CoMoO_4$/bamboo Charcoal Hybrid Material for High-energy-density and High Cycling Stability Supercapacitors. *Dalton Trans.* **2020**, *49*, 10799–10807.
178. Zhou, E.M.; Tian, L.L.; Cheng, Z.F.; Fu, C.P. Design of NiO Flakes@$CoMoO_4$ Nanosheets Core-Shell Architecture on Ni Foam for High-Performance Supercapacitors. *Nanoscale Res. Lett.* **2019**, *14*, 211.
179. Lv, Y.M.; Liu, A.F.; Che, H.W.; Mu, J.B.; Guo, Z.C.; Zhang, X.L.; Bai, Y.M.; Zhang, Z.X.; Wang, G.S.; Pei, Z.Z. Three-dimensional Interconnected $MnCo_2O_4$ nanosheets@$MnMoO_4$ Nanosheets Core-shell Nanoarrays on Ni foam for High-performance Supercapacitors. *Chem. Eng. J.* **2018**, *336*, 64–73.
180. Wan, L.; Liu, J.X.; Li, X.; Zhang, Y.; Chen, J.; Du, C.; Xie, M.J. Fabrication of Core-shell $NiMoO_4$@MoS_2 Nanorods for High-performance Asymmetric Hybrid Supercapacitors. *Int. J. Hydrogen Energy* **2020**, *45*, 4521–4533.
181. Xuan, H.C.; Li, H.S.; Yang, J.; Liang, X.H.; Xie, Z.G.; Han, P.D.; Wu, Y.C. Rational Design of Hierarchical Core-shell Structured $CoMoO_4$@CoS Composites on Reduced Graphene Oxide for Supercapacitors with Enhanced Electrochemical Performance. *Int. J. Hydrogen Energy* **2020**, *45*, 6024–6035.
182. Hussain, I.; Ali, A.; Lamiel, C.; Mohamed, S.G.; Sahoo, S.; Shim, J.J. A 3D Walking Palm-like Core–shell $CoMoO_4$@$NiCo_2S_4$@Nickel Foam Composite for High-performance Supercapacitors. *Dalton Trans.* **2019**, *48*, 3853–3861. [CrossRef] [PubMed]
183. Zhang, X.Y.; Fu, Q.G.; Huang, H.M.; Wei, L.; Guo, X. Silver-quantum-dot-modified MoO_3 and MnO_2 paper-like Freestanding Films for Flexible solid-state Asymmetric Supercapacitors. *Small* **2019**, *15*, 1805235. [CrossRef]
184. Shen, T.; Yang, L.P.; Pam, M.E.; Shi, Y.M.; Yang, H.Y. Quantum Dot-carbonaceous Nanohybrid Composites: Preparation and Application in Electrochemical Energy storage. *J. Mater. Chem. A* **2020**, *8*, 22488–22506. [CrossRef]
185. Manikandan, A.; Chen, Y.Z.; Shen, C.C.; Sher, C.W.; Kuo, H.C.; Chueh, Y.L. A Critical Review on Two-dimensional Quantum Dots (2D QDs): From Synthesis toward Applications in Energy and Optoelectronics. *Prog. Quant. Electron.* **2019**, *68*, 100226. [CrossRef]
186. Xu, Q.; Cai, W.; Li, W.; Sreeprasad, T.S.; He, Z.Y.; Ong, W.-J.; Li, N. Two-dimensional Quantum Dots: Fundamentals, Photoluminescence Mechanism and their Energy and Environmental Applications. *Mater. Today Energy* **2018**, *10*, 222–240. [CrossRef]
187. Ji, Z.Y.; Ma, D.W.; Dai, W.Y.; Liu, K.; Shen, X.P.; Zhu, G.X.; Nie, Y.J.; Pasang, D.; Yuan, A.H. Anchoring Nitrogen-doped Carbon Quantum Dots on Nickel Carbonate Hydroxide Nanosheets for Hybrid Supercapacitor Applications. *J. Colloid Interface Sci.* **2021**, *590*, 614–621. [CrossRef]
188. Duan, H.Y.; Wang, T.; Wu, X.Y.; Su, Z.Y.; Zhuang, J.; Liu, S.L.; Zhu, R.M.; Chen, C.Y.; Pang, H. CeO_2 Quantum Dots Doped Ni-Co Hydroxide Nanosheets for Ultrahigh Energy Density Asymmetric Supercapacitors. *Chin. Chem. Lett.* **2020**, *31*, 2330–2332. [CrossRef]
189. Samuei, S.; Rezvani, Z.; Shomali, A.; Ulker, E.; Karadas, F. Preparation and Capacitance Properties of Graphene Quantum Dot/NiFe-Layered Double-Hydroxide Nanocomposite. *Eur. J. Inorg. Chem.* **2021**, *2021*, 258–266. [CrossRef]
190. Zhu, Y.R.; Wu, Z.B.; Jing, M.J.; Hou, H.S.; Yang, Y.C.; Zhang, Y.; Yang, X.M.; Song, W.X.; Jia, X.N.; Ji, X.B. Porous $NiCo_2O_4$ Spheres Tuned through Carbon Quantum Dots Utilised as Advanced Materials for an Asymmetric Supercapacitor. *J. Mater. Chem. A* **2015**, *3*, 866–877.
191. Zhang, M.W.; Liu, W.W.; Liang, R.L.; Tjandra, R.; Yu, A.P. Graphene Quantum Dot Induced Tunable Growth of Nanostructured $MnCo_2O_{4.5}$ Composites for High-performance Supercapacitors. *Sustain. Energy Fuels* **2019**, *3*, 2499–2508. [CrossRef]
192. Zhang, X.Y.; Li, Z.; Yu, Z.Y.; Wei, L.; Guo, X. Mesoporous $NiMoO_4$ Microspheres Decorated by Ag Quantum Dots as Cathode Material for Asymmetric Supercapacitors: Enhanced Interfacial Conductivity and Capacitive Storage. *Appl. Surf. Sci.* **2020**, *505*, 144513. [CrossRef]